(h2)-CaP and acidic (h3)-CaP in bladder tissues were analysed by reverse-transcription-PCR. Our results shown in Fig. 1*D* demonstrate that loss of h1-CaP does not affect the expression of h2- or h3-CaP isoforms.

Loss of SM-B and h1-CaP did not affect the smooth muscle morphology

To determine whether loss of h1-CaP in SM-B null mice results in any structural abnormalities, histopathological analysis was carried out. Bladder tissues from *smb−/−* and dKO mice were fixed in 10% neutral buffered formalin, dehydrated through a gradient of alcohols, embedded in paraffin, and sectioned and stained with haematoxylin and eosin as described earlier (Karagiannis *et al.* 2003). Results in Fig. 2 show no significant difference between *smb−/−* and dKO mice bladder muscle. The smooth muscle morphology and orientation were normal and similar between single and dKO mice. These results suggest that loss of both SM-B myosin and h1-CaP did not alter smooth muscle structure and development.

Loss of SM-B and h1-CaP did not affect the myosin heavy and light chain isoform expression

To determine whether loss of both SM-B and h1-CaP proteins induced changes in myosin protein expression or isoform switching, Western blot analysis was carried out using protein extracts prepared from bladder and mesenteric vessels. Our results indicate that ablation of h1-CaP did not affect the level of SM1 (WT = 100%, *smb−/−* = 101 ± 2.2%, dKO = 99.8 ± 1.6%; $P > 0.05$), SM2 (WT = 100%, *smb−/−* = 104 ± 1.9%, dKO = 102 ± 1.6%; $P > 0.05$), LC_{17} (WT = 100%, *smb−/−* = 105 ± 3.0%, dKO = 101 ± 5.0%; $P > 0.05$) and LC_{20} (WT = 100%, *smb−/−* = 100 ± 4.6%, dKO = 103 ± 4.4%; $P > 0.05$) proteins in the dKO mice bladder (Fig. 3*A*). Similar results were also obtained with mesenteric vessels (Fig. 3*B*).

Smooth muscle α-actin levels are decreased in the dKO bladder

Western blot analysis revealed that smooth muscle α-actin levels are ~40% down-regulated in the dKO bladder (Fig. 4*A* and *B*) and mesenteric vessels (Fig. 5*A* and *B*). These data are consistent with a previous report on the down-regulation of smooth muscle α-actin expression in h1-CaP single knockout bladder (Matthew *et al.* 2000). The γ-actin and non-muscle β-actin protein levels were unchanged in both bladder (Figs 1*A* and 4*A*) and mesenteric vessels (Figs 1*B* and 5*A*) of dKO mice, indicating that ablation of h1-CaP did not affect the expression of other actin isoforms.

Smooth muscle-specific h-CaD has been shown to be down-regulated in the *smb−/−* mice (Babu *et al.* 2004). To determine if loss of h1-CaP affects CaD levels, Western blot analysis was carried out using smooth muscle-specific h-CaD antibody. Our results show that h-CaD protein levels are decreased in the *smb−/−* bladder (Fig. 4*A* and *C*) and mesenteric vessels (Fig. 5*A* and *C*) as reported earlier (Babu *et al.* 2004). Interestingly, ablation of CaP restores the h-CaD expression in the dKO bladder (Fig. 4*A* and *C*) as well as in the mesenteric vessels (Fig. 5*A* and *C*) and its level is significantly higher than the wild-type tissues.

Contractile properties of dKO mice bladder

To determine how loss of CaP affects smooth muscle contractility in *smb−/−* bladder, we compared shortening velocity (V_{max}) and force generation between *smb−/−* and dKO mice bladder as described earlier (Karagiannis *et al.* 2003). Steady-state forces between WT and *smb−/−* bladder were not

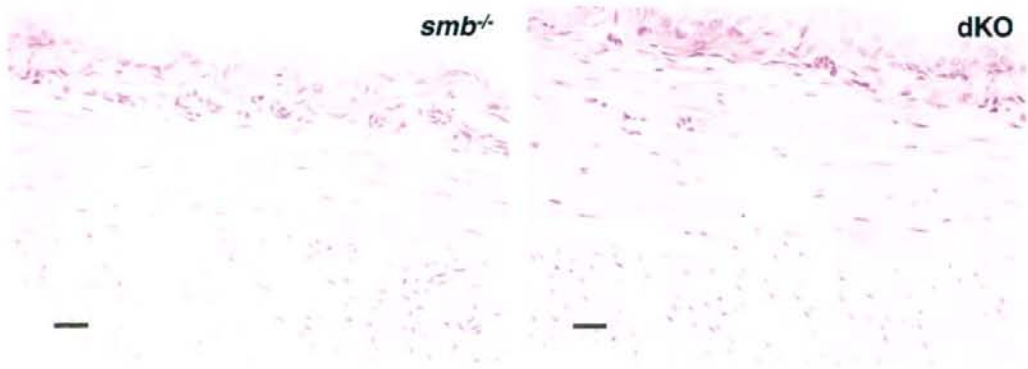

Figure 2. Histological staining of SM-B null and dKO mice bladder
Bladder tissue from *smb−/−* (left panel) and dKO mice (right panel) was fixed with formalin and stained with haematoxylin and eosin. Scale bar, 10 μm.

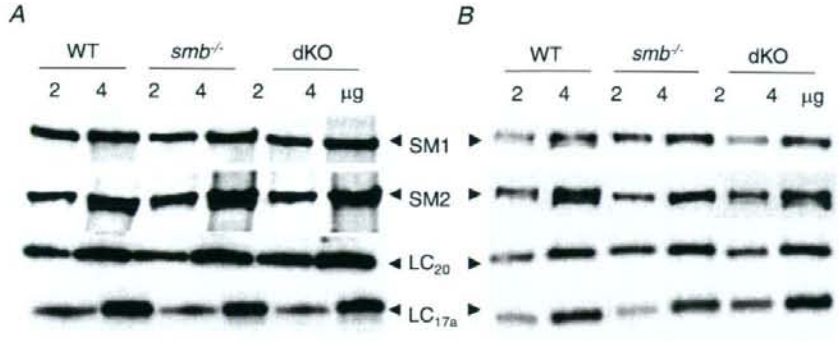

Figure 3. Expression of myosin heavy and light chain isoforms
Two different concentrations (2 and 4 μg) of total protein extracts prepared from *smb−/−* and dKO bladders (*A*) and mesenteric vessels (*B*) were separated on 5% (for SM1 and SM2) or 14% SDS-PAGE (for LC_{20} and LC_{17}) and immunoprobed with specific antibodies. Expression levels of myosin isoforms are unaltered in the dKO bladder. Signals were quantified by densitometry scanning. Data are representative of 3 independent experiments.

statistically different ($WT = 9.9 \pm 0.7$ mN mm^{-2} *versus* *smb−/−* $= 8.9 \pm 0.7$ mN mm^{-2}); however, the steady-state force was significantly increased in the dKO bladder (dKO $= 12.5 \pm 0.5$ mN mm^{-2}) and was significantly higher than WT (Fig. 6). As reported earlier (Karagiannis *et al.* 2003), the velocity of shortening was significantly decreased in the *smb−/−* bladder ($WT = 0.22 \pm 0.4$ ML s^{-1} ($n = 10$) *versus* *smb−/−* $= 0.18 \pm 0.1$ muscle lengths (ML) s^{-1} ($n = 7$)). Interestingly, V_{max} in the dKO bladder (dKO $= 0.24 \pm 0.2$ ($n = 9$)) was no different to that of WT bladder, but significantly higher than that observed in the SM-B null mice.

Contractile properties of mesenteric vessels

As summarized in Table 1, there were no differences observed in all three groups in vessel diameter at 50 mmHg

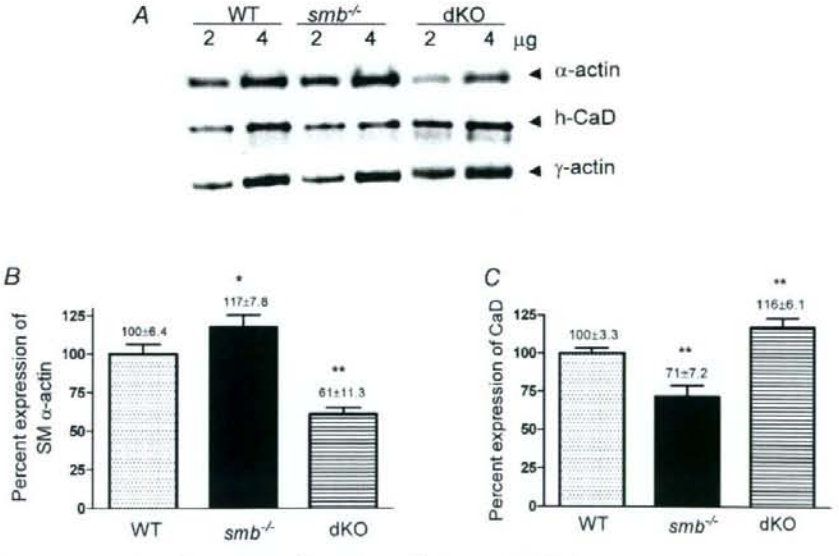

Figure 4. Expression of smooth muscle α-actin and h-CaD in dKO bladder
A, representative Western blots showing the expression of α-actin, γ-actin and h-CaD expression in dKO bladder. γ-Actin levels are unchanged between the three groups. *B* and *C*, bar graphs showing the percentage expression of smooth muscle α-actin and CaD proteins in the dKO bladder. Smooth muscle α-actin is down-regulated ~40% (*B*) whereas h-CaD is up-regulated (*C*) in the dKO bladder. *Not significantly different from WT. **Significantly different from the other two groups.

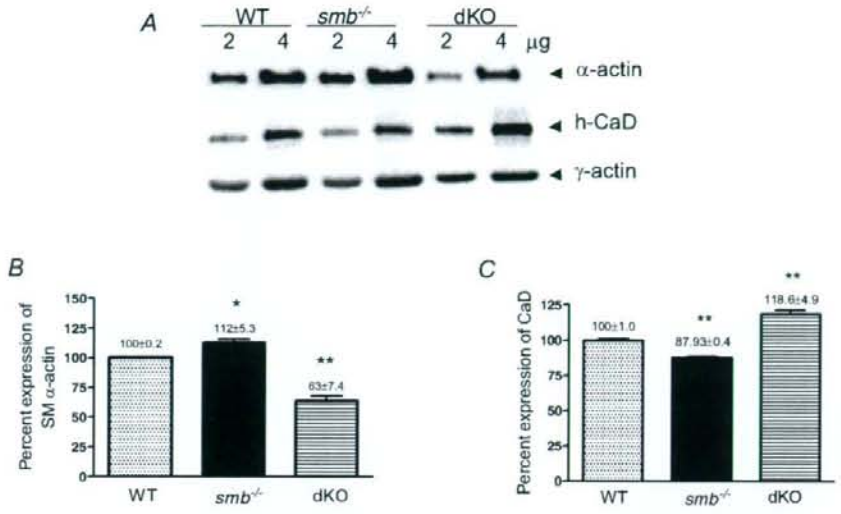

Figure 5. Expression of smooth muscle α-actin and h-CaD in dKO mesenteric vessels
A, representative Western blots showing the expression of α-actin, γ-actin and h-CaD expression in dKO mesenteric vessels. γ-Actin levels are unchanged between the three groups. *B* and *C*, bar graphs showing the percentage expression of smooth muscle α-actin and h-CaD proteins. Smooth muscle α-actin is down-regulated ~40% (*B*) whereas h-CaD is up-regulated (*C*) in the dKO mesenteric vessels. *Not significantly different from WT. **Significantly different from other two groups.

in a relaxing solution containing papaverine (0.1 mM) in the extent of maximal vasoconstriction to an activation cocktail containing phenylephrine (10 μM) and potassium (120 mM) or in the equivalent maximal reductions in lumen diameter (approximately 80%). Half-time ($T_{1/2}$) to maximal constriction was significantly increased in both knockout (*smb*−/− and dKO) groups, indicating decreased shortening velocity, as was the normalized slope of constriction (percentage diameter change per second) in vessels from both the *smb*−/− and dKO animals (Table 1).

Relative to vessels from the *smb*−/− animals, the pressure at which forced dilatation occurred was significantly increased in the dKO mesenteric vessels, and reached the levels of WT control vessels (Table 1). Forced dilatation (FD; used in the present study) is an indirect measure of maximal force production, and is defined as the point at which transmural pressure overcomes the ability of vascular smooth muscle to produce an adequate counterforce to circumferential tension produced by the intraluminal pressure. These data showing enhanced force production by mesenteric artery smooth muscle from dKO *versus smb*−/− animals are in general agreement with those obtained from bladder smooth muscle and described above.

Discussion

The major goal of the current study was to determine the functional significance of h1-CaP up-regulation in

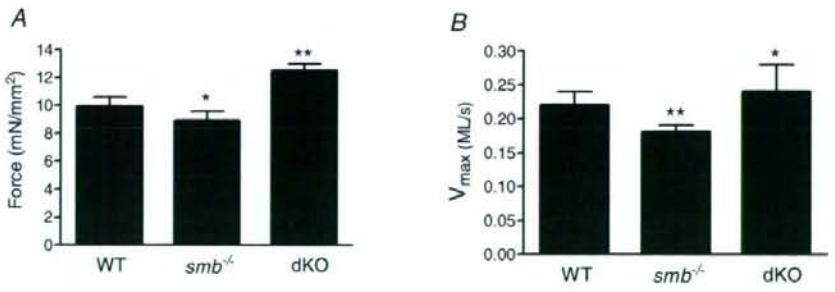

Figure 6. Functional measurements on *smb*−/− and dKO bladder
A, force; *B*, V_{max}. Data are means ± S.E.M. ($P < 0.05$). *Not significantly different from WT. **Significantly different from the other two groups.

Table 1. Contractile properties of mesenteric vessels

Experimental parameters	WT ($n = 5$)	*smb−/−* ($n = 6$)	dKO ($n = 5$)
Maximal relaxed lumen diameter at 50 mmHg (μm)	196 ± 17.6	198 ± 16.5	200 ± 10.3
Maximal constriction (% decrease in lumen diameter)	79 ± 3.3	80 ± 1.6	79 ± 1.5
Time to 50% constriction (s)	4.2 ± 0.49†	5.2 ± 0.68*	5.6 ± 0.58*
Slope of constriction (normalized: % change in lumen diameter s^{-1})	12.8 ± 1.45†	10.5 ± 1.33*	9.6 ± 1.37*
Forced dilatation pressure (mmHg)	204 ± 6.7†	183 ± 7.8*	202 ± 8.2†

Vessels were constricted with an activation cocktail containing phenylephrine (10 μM) and potassium (124 mM). Different symbols (†,*) indicate significant differences ($P < 0.05$) between groups; identical symbols are not significantly different from each other. All comparisons performed by two-way ANOVA.

SM-B null mice (Babu *et al.* 2004). To critically asses the role of h1-CaP in the contractile function of SM-B null smooth muscles, we ablated h1-CaP in the SM-B null background by crossing h1-CaP and SM-B single knockout mice. The key findings of this study are as follows. (1) Ablation of CaP in the SM-B null mice bladder resulted in increased V_{max} and steady-state force generation. (2) In mesenteric vessels, the maximal force as measured by forced dilatation was increased in the dKO mice, and the higher maximal force allows the vessel to shorten faster under a load. The shortening velocity, however, was decreased in both *smb−/−* and dKO vessels. (3) Interestingly, these functional changes were observed with a decrease in smooth muscle α-actin levels and an increase in caldesmon levels.

We have previously shown that switching of SM-B to SM-A myosin in a SM-B null mouse model resulted in decreased velocity of shortening (Babu *et al.* 2001; Karagiannis *et al.* 2003) and increased expression of h1-CaP (Babu *et al.* 2004). The available data strongly suggest that h1-CaP is involved in the regulation of actin–myosin interaction and therefore the kinetics of smooth muscle contractility (Takahashi & Yamamura, 2003). Ablation of h1-CaP significantly increases the unloaded shortening velocity in phasic smooth muscle tissues such as bladder and vas deferens (Matthew *et al.* 2000; Takahashi *et al.* 2000). These findings taken together suggest that the up-regulation of h1-calponin could negatively influence the velocity of shortening in SM-B null mice. Therefore, the dKO mouse model lacking both h1-CaP and SM-B myosin provide us with an excellent model to determine the functional significance of h1-CaP up-regulation in SM-B null mice. In dKO mice, loss of both h1-CaP and SM-B myosin proteins does not affect survival or cause any overt smooth muscle pathology as observed in the individual knockout animals (Yoshikawa *et al.* 1998; Babu *et al.* 2001). Loss of h1-CaP is not compensated by other CaP isoforms (Fig. 1C) and consistent with the previous studies on h1-CaP single knockout (Yoshikawa *et al.* 1998). Interestingly, loss of CaP in the SM-B null background is associated with ~40% reduction in the smooth muscle α-actin levels. However, loss of h1-CaP does not affect the β- and γ-actin isoforms (Figs 1, 4 and 5). These changes are also consistent with changes associated with CaP single knockout mice (Matthew *et al.* 2000) and indicate the preservation of the CaP null phenotype in the dKO mice.

As previously reported, the loss of SM-B myosin does not alter the unitary force generation in bladder muscle compared to the WT bladder (Karagiannis *et al.* 2003, 2004). However, ablation of h1-CaP resulted in increased steady-state force generation in the SM-B null mice. Increased steady-state force generation under conditions where LC_{20} were maximally, irreversibly phosphorylated, and in the absence of structural changes (as observed by histology) suggests that h1-CaP may play a role in modulating bladder smooth muscle contractility. However, these results differ from the previous report using h1-CaP single knockout mice, which showed no significant difference in force development in the skinned bladder muscles between WT and h1-CaP null mice (Matthew *et al.* 2000), and rather decreased force production in intact vas deferens and aortic smooth muscles (Takahashi *et al.* 2000; Fujishige *et al.* 2002). The unexpected increase in force in the dKO bladder could be due to the complete replacement of SM-B by the SM-A myosin isoform in the bladder and/or other compensatory changes yet to be analysed.

In agreement with previous results, the WT bladder shortened at a rate 20% faster than the *smb−/−* bladder (Karagiannis *et al.* 2003). The V_{max}, however, was significantly increased in the dKO bladder as compared to *smb−/−* bladder, under conditions in which the levels of myosin thiophosphorylation were similar. These results indicate that myosin light chain phosphorylation does not contribute for the observed velocity changes. A similar increase in V_{max} has been reported for h1-CaP single knockout (Matthew *et al.* 2000; Takahashi *et al.* 2000). We have previously shown that the 7 amino acid insert regulates the earlier rate-limiting step including nucleotide binding and inorganic phosphate release (Karagiannis *et al.* 2003) whereas CaP is proposed to regulate the later steps in the cross-bridge cycle such as dissociation of high-affinity cross-bridges from actin, by binding to actin (EL-Mezgueldi & Marston, 1996; Takahashi & Yamamura, 2003). Therefore, both h1-CaP and SM-B myosin could

affect the cross-bridge cycling and V_{max} but at different kinetic steps. Taken together our studies suggest that up-regulation of h1-CaP in the SM-B null mice may be a compensatory alteration to maintain a reduced level of cross-bridge cycling over time in the absence of SM-B myosin. However, reduction in the smooth muscle α-actin levels and increase in h-CaD levels suggest that changes in other contractile and regulatory proteins may also contribute to the altered contractile properties observed in the dKO bladder.

In addition to bladder, the contractile properties of mesenteric vessels were determined in the dKO mice. We have previously reported that SM-B myosin is expressed heterogeneously in the mesenteric vessels and contributes to their unique mechanical properties (Babu *et al.* 2004). In that study, we also found that loss of SM-B myosin resulted in increased force generation under isometric conditions (using wire-mounted vessel rings) in response to phenylephrine + potassium (Babu *et al.* 2004). In the present study, which used a more physiological pressurized vessel approach, maximal constriction to an activation cocktail containing high potassium (124 mM) and phenylephrine (10 μM) was similar in all treatment groups. Since the vessel is studied as an intact unit, the maximal extent of constriction, measured as the reduction in lumen diameter from a fully relaxed state, may be limited by other factors, e.g. cell–matrix interactions, rather than simply maximal force generation.

The (1) increased half-time to maximal constriction, and (2) reduced normalized slope of constriction observed in mesenteric vessels of both *smb−/−* and dKO mouse models, both suggest decreased shortening velocity of smooth muscle. These findings are consistent with our previous studies showing decreased shortening velocity in the mesenteric vessels with SM-B deficiency (Babu *et al.* 2001, 2004), and indicate that changes in h1-CaP do not seem to be the underlying cause for the altered kinetics in this type of smooth muscle. Another study using rat portal vein also showed that the maximal velocity of vascular smooth muscle shortening was independent of h1-CaP expression (Facemire *et al.* 2000).

The significantly reduced forced dilatation pressure in vessels from the *smb−/−* but not dKO mice was an unexpected finding that suggests that the modulatory effect of calponin on vascular smooth muscle (VSM) contractility may be influenced by (1) the extent of VSM activation, (2) spatial events such as the degree of actin–myosin overlap (the length–tension relationship), and (3) the nature of the distending force acting upon the vascular wall. All three possibilities derive from our use of the more physiological pressurized vessel methodology in this study, since earlier work used the isometric wire-mounted approaches in which vessels are stretched to a fixed length prior to activation and therefore unable to shorten in response to activation. In the pressurized vessel, as in the body, activation results in constriction, which is a reflection of smooth muscle shortening. This may have implications for the spatial relationship between actin, myosin and calponin, and thereby alter the nature of thin filament regulation, as there were no detectable differences in myosin heavy and light chain isoform expression. Further, in pressurized vessels, the force experienced by the vascular wall is true transmural pressure, which has a radial as well as a circumferential component that may influence the distribution of intramural stress. Although it was beyond the scope of this study to differentiate the ultrastructural/spatial *versus* biomechanical components of the response, these elements deserve consideration in future studies. Finally, although the velocity data were consistent with previous findings in mesenteric vessels (Babu *et al.* 2004) and in bladder smooth muscle (this study), it should be noted that, in arteries, the importance of shortening velocity *in vivo* is questionable, while the production and maintenance of force is essential to the maintenance of vascular tone and, thereby, peripheral resistance, blood pressure and normal organ perfusion. This differs from the bladder, whose proper function is dependent on smooth muscle shortening for effective micturition. Thus, it is not unreasonable to expect differences in the nature of h1-CaP regulation based on physiological function. Based on the results of our studies, h1-CaP appears to be a key regulator of both bladder and vascular smooth muscle contractility, although its precise modulatory role may clearly vary with smooth muscle tissue type and function.

References

Arner A, Lofgren M & Morano I (2003). Smooth, slow and smart muscle motors. *J Muscle Res Cell Motil* **24**, 165–173.

Babu GJ, Loukianov E, Loukianova T, Pyne GJ, Huke S, Osol G, Low RB, Paul RJ & Periasamy M (2001). Loss of SM-B myosin affects muscle shortening velocity and maximal force development. *Nat Cell Biol* **3**, 1025–1029.

Babu GJ, Pyne GJ, Zhou Y, Okwuchukuasanya C, Brayden JE, Osol G, Paul RJ, Low RB & Periasamy M (2004). Isoform switching from SM-B to SM-A myosin results in decreased contractility and altered expression of thin filament regulatory proteins. *Am J Physiol Cell Physiol* **287**, C723–C729.

Babu GJ, Warshaw DM & Periasamy M (2000). Smooth muscle myosin heavy chain isoforms and their role in muscle physiology. *Microsc Res Tech* **50**, 532–540.

D'Angelo G & Osol G (1993). Regional variation in resistance artery diameter responses to α-adrenergic stimulation during pregnancy. *Am J Physiol Heart Circ Physiol* **264**, H78–H85.

DiSanto ME, Cox RH, Wang Z & Chacko S (1997). NH2-terminal-inserted myosin II heavy chain is expressed in smooth muscle of small muscular arteries. *Am J Physiol Cell Physiol* **272**, C1532–C1542.

EL-Mezgueldi M & Marston SB (1996). The effects of smooth muscle calponin on the strong and weak myosin binding sites of F-actin. *J Biol Chem* **271**, 28161–28167.

Facemire C, Brozovich FV & Jin JP (2000). The maximal velocity of vascular smooth muscle shortening is independent of the expression of calponin. *J Muscle Res Cell Motil* **21**, 367–373.

Fujishige A, Takahashi K & Tsuchiya T (2002). Altered mechanical properties in smooth muscle of mice with a mutated calponin locus. *Zool Sci* **19**, 167–174.

Haase H & Morano I (1996). Alternative splicing of smooth muscle myosin heavy chains and its functional consequences. *J Cell Biochem* **60**, 521–528.

Haeberle JR (1994). Calponin decreases the rate of cross-bridge cycling and increases maximum force production by smooth muscle myosin in an in vitro motility assay. *J Biol Chem* **269**, 12424–12431.

Horiuchi KY & Chacko S (1991). The mechanism for the inhibition of actin-activated ATPase of smooth muscle heavy meromyosin by calponin. *Biochem Biophys Res Commun* **176**, 1487–1493.

Itoh T, Suzuki S, Suzuki A, Nakamura F, Naka M & Tanaka T (1994). Effects of exogenously applied calponin on Ca^{2+}-regulated force in skinned smooth muscle of the rabbit mesenteric artery. *Pflugers Arch* **427**, 301–308.

Jaworowski A, Anderson KI, Arner A, Engstrom M, Gimona M, Strasser P & Small JV (1995). Calponin reduces shortening velocity in skinned taenia coli smooth muscle fibres. *FEBS Lett* **365**, 167–171.

Karagiannis P, Babu GJ, Periasamy M & Brozovich FV (2003). The smooth muscle myosin seven amino acid heavy chain insert's kinetic role in the crossbridge cycle for mouse bladder. *J Physiol* **547**, 463–473.

Karagiannis P, Babu GJ, Periasamy M & Brozovich FV (2004). Myosin heavy chain isoform expression regulates shortening velocity in smooth muscle: studies using an SMB KO mouse line. *J Muscle Res Cell Motil* **25**, 149–158.

Karagiannis P & Brozovich FV (2003). The kinetic properties of smooth muscle: how a little extra weight makes myosin faster. *J Muscle Res Cell Motil* **24**, 157–163.

Kelley CA, Takahashi M, Yu JH & Adelstein RS (1993). An insert of seven amino acids confers functional differences between smooth muscle myosins from the intestines and vasculature. *J Biol Chem* **268**, 12848–12854.

Lauzon AM, Trybus KM & Warshaw DM (1998*a*). Molecular mechanics of two smooth muscle heavy meromyosin constructs that differ by an insert in the motor domain. *Acta Physiol Scand* **164**, 357–361.

Lauzon AM, Tyska MJ, Rovner AS, Freyzon Y, Warshaw DM & Trybus KM (1998*b*). A 7-amino-acid insert in the heavy chain nucleotide binding loop alters the kinetics of smooth muscle myosin in the laser trap. *J Muscle Res Cell Motil* **19**, 825–837.

Lofgren M, Fagher K, Wede OK & Arner A (2002). Decreased shortening velocity and altered myosin isoforms in guinea-pig hypertrophic intestinal smooth muscle. *J Physiol* **544**, 707–714.

Matthew JD, Khromov AS, McDuffie MJ, Somlyo AV, Somlyo AP, Taniguchi S & Takahashi K (2000). Contractile properties and proteins of smooth muscles of a calponin knockout mouse. *J Physiol* **529**, 811–824.

Matthew JD, Khromov AS, Trybus KM, Somlyo AP & Somlyo AV (1998). Myosin essential light chain isoforms modulate the velocity of shortening propelled by nonphosphorylated cross-bridges. *J Biol Chem* **273**, 31289–31296.

Morgan KG & Gangopadhyay SS (2001). Invited review: cross-bridge regulation by thin filament-associated proteins. *J Appl Physiol* **91**, 953–962.

Rovner AS, Freyzon Y & Trybus KM (1997). An insert in the motor domain determines the functional properties of expressed smooth muscle myosin isoforms. *J Muscle Res Cell Motil* **18**, 103–110.

Siegman MJ, Butler TM, Mooers SU, Trinkle-Mulcahy L, Narayan S, Adam L, Chacko S, Haase H & Morano I (1997). Hypertrophy of colonic smooth muscle: contractile proteins, shortening velocity, and regulation. *Am J Physiol Gastrointest Liver Physiol* **272**, G1571–G1580.

Somlyo AV, Khromov AS, Webb MR, Ferenczi MA, Trentham DR, He ZH, Sheng S, Shao Z & Somlyo AP (2004). Smooth muscle myosin: regulation and properties. *Philos Trans R Soc Lond B Biol Sci* **359**, 1921–1930.

Somlyo AV, Matthew JD, Wu X, Khromov AS & Somlyo AP (1998). Regulation of the cross-bridge cycle: the effects of MgADP, LC17 isoforms and telokin. *Acta Physiol Scand* **164**, 381–388.

Takahashi K & Yamamura H (2003). Studies and perspectives of calponin in smooth muscle regulation and cancer gene therapy. *Adv Biophys* **37**, 91–111.

Takahashi K, Yoshimoto R, Fuchibe K, Fujishige A, Mitsui-Saito M, Hori M, Ozaki H, Yamamura H, Awata N, Taniguchi S, Katsuki M, Tsuchiya T & Karaki H (2000). Regulation of shortening velocity by calponin in intact contracting smooth muscles. *Biochem Biophys Res Commun* **279**, 150–157.

Uyama Y, Imaizumi Y, Watanabe M & Walsh MP (1996). Inhibition by calponin of isometric force in demembranated vascular smooth muscle strips: the critical role of serine-175. *Biochem J* **319**, 551–558.

Winder SJ, Allen BG, Clement-Chomienne O & Walsh MP (1998). Regulation of smooth muscle actin–myosin interaction and force by calponin. *Acta Physiol Scand* **164**, 415–426.

Yoshikawa H, Taniguchi SI, Yamamura H, Mori S, Sugimoto M, Miyado K, Nakamura K, Nakao K, Katsuki M, Shibata N & Takahashi K (1998). Mice lacking smooth muscle calponin display increased bone formation that is associated with enhancement of bone morphogenetic protein responses. *Genes Cells* **3**, 685–695.

Ackowledgements

This work was supported by American Heart Association Grant 0365173B (to G.J.B.), National Heart, Lung, and Blood Institute Grant HL-38355-17 (to M.P.) and HL-44181 (to F.V.B.).

Available online at www.sciencedirect.com
ScienceDirect
Biochemical and Biophysical Research Communications 350 (2006) 315–321
BBRC
www.elsevier.com/locate/ybbrc

Loss of HB-EGF in smooth muscle or endothelial cell lineages causes heart malformation

Daisuke Nanba [a,1], Yumi Kinugasa [a,1], Chie Morimoto [a], Michiko Koizumi [a], Hisako Yamamura [c], Katsuhito Takahashi [c], Nobuyuki Takakura [d], Eisuke Mekada [e], Koji Hashimoto [b], Shigeki Higashiyama [a,f,*]

[a] *Department of Biochemistry and Molecular Genetics, Ehime University Graduate School of Medicine, Shitsukawa, To-on, Ehime 791-0295, Japan*
[b] *Department of Dermatology, Ehime University Graduate School of Medicine, Shitsukawa, To-on, Ehime 791-0295, Japan*
[c] *Department of Medicine, Osaka Medical Center for Cancer and Cardiovascular Diseases, Osaka 537-8511, Japan*
[d] *Department of Signal Transduction, Research Institute for Microbial Diseases, Osaka University, Osaka 565-0871, Japan*
[e] *Department of Cell Biology, Research Institute for Microbial Diseases, Osaka University, Osaka 565-0871, Japan*
[f] *PRESTO, JST, Japan*

Received 22 August 2006
Available online 22 September 2006

Abstract

Epidermal growth factor (EGF) and ErbB family molecules play a role in heart development and function. To investigate the role of EGF family member, heparin-binding EGF-like growth factor (HB-EGF) in heart development, smooth muscle and endothelial cell lineage-specific HB-EGF knockout mice were generated using the Cre/*loxP* system in combination with the *SM22α* or *TIE2* promoter. HB-EGF knockout mice displayed enlarged heart valves, and over half of these mice died during the first postnatal week, while survivors showed cardiac hypertrophy. These results suggest that expression of HB-EGF in smooth muscle and/or endothelial cell lineages is essential for proper heart development and function in mice.

Keywords: Cardiac hypertrophy; Conditional knockout; HB-EGF; Heart valves; Heart failure

Heparin-binding EGF-like growth factor (HB-EGF) is a member of the EGF family of molecules that was first identified in the conditioned media of macrophage-like U-937 cells [1]. HB-EGF is initially synthesized as a type I transmembrane precursor protein (proHB-EGF) that is subsequently enzymatically cleaved to release a soluble form of HB-EGF [1,2]. Further, HB-EGF acts as a mitogen in many different cell types and is involved in a variety of physiological and pathological processes [3–5].

Two independent studies have reported that over half of HB-EGF-null mice die before weaning and that survivors have dysfunctional hearts with grossly enlarged ventricular chambers and reduced life spans [6,7]. Moreover, studies have described the development of enlarged cardiac valves in HB-EGF-deficient mice. This heart valve enlargement has also been observed in EGF receptor (EGFR)-null mice with a CD1 background, in mice with a mutant EGFR (*waved-2*) [8], and in disintegrin and metalloprotease (ADAM) 17-null mice [7], which is a sheddase of proHB-EGF [9,10]. These results indicate that ectodomain shedding of proHB-EGF and subsequent EGFR activation induced by released HB-EGF are crucial for heart valve formation in developmental process as well as development of cardiac hypertrophy in pathological process [11]. However, it is not clear in which of the specific heart cell types (e.g., cardiac myocytes, endothelial cells, and fibroblasts) that HB-EGF expression is required for proper heart development and function.

* Corresponding author. Fax: +81 89 960 5256.
E-mail address: shigeki@m.ehime-u.ac.jp (S. Higashiyama).
[1] These authors contributed equally to this work.

0006-291X/$ - see front matter © 2006 Elsevier Inc. All rights reserved.
doi:10.1016/j.bbrc.2006.09.060

To address this issue, the present study utilized the Cre/*loxP* recombination system for spatiotemporal *HB-EGF* gene ablation. The system generally requires cross-mating of two lines of genetically manipulated mice. One line of mice carries alleles with the *HB-EGF* gene flanked by *loxP* sites [6], and the other line contains a Cre transgene in which the expression of Cre is controlled by *SM22α* or *TIE2* promoter [12,13]. Recombination between the two *loxP* sites in the mated mice results in the catalysis of a deletion of the region flanked by the *loxP* sites (i.e., Cre-dependent transgene expression).

The *SM22α* gene encodes a calponin-related protein that is expressed specifically in adult smooth muscle [14–17]. During mouse embryogenesis, *SM22α* is expressed in cardiac muscle, smooth muscle, and skeletal muscle cells, but becomes restricted to smooth muscle lineages at late embryonic stages and throughout adulthood [18]. The *TIE2* gene encodes an angiopoietin receptor, which is a member of the receptor tyrosine kinase family [19,20]. *TIE2* expression is detected as the first endothelial cells arise, remains positive in endothelial cells throughout development, and is detectable in virtually all endothelial cells of adult tissues [19,21,22].

In this study, we generated smooth muscle and endothelial cell lineage specific HB-EGF knockout mice using Cre/*loxP* system in combination with the *SM22α* and *TIE2* promoter, and demonstrated that HB-EGF in smooth muscle and endothelial lineages was essential for heart development and function.

Materials and methods

Generation of HB-EGF conditional knockout mice using a gene targeting Cre/loxP strategy. Mice with *HB-EGF* gene flanked by *loxP* sites ($HB^{lox/lox}$) were generated as previously described [6]. Homozygous $HB^{lox/lox}$ mice were bred with *SM22α* or *TIE2* promoter-driven Cre-recombinase transgenic mice [12,13] to generate SM22α-Cre:$HB^{lox/WT}$ or TIE2-Cre:$HB^{lox/WT}$ mice. The obtained mice were bred with $HB^{lox/lox}$ mice to generate SM22α-Cre:$HB^{lox/lox}$ (SM22α-Cre:$HB^{-/-}$) or TIE2-Cre:$HB^{lox/lox}$ (TIE2-Cre:$HB^{-/-}$) mice. The genotype of each mouse was confirmed by PCR. Primers are shown in Table 1.

Table 1
Primer sequences for PCR

Wild-type *HB-EGF* (forward)	5′-CATGATGCTCCAGTGAGTAGGCTCTGATTAC-3′
Wild-type *HB-EGF* (reverse)	5′-AGGGCAAGATCATGTGTCCTGCCTCAAGCC-3′
loxP HB-EGF (forward)	5′-ATGGGATCGGCCATTGAACA-3′
loxP HB-EGF (reverse)	5′-GAAGAACTCGTCAAGAAGGC-3′
Cre recombinase (forward)	5′-TTACCGGTCGATGCAACGAGTGATG-3′
Cre recombinase (reverse)	5′-TTCCATGAGTGAACGAACCTGGTCG-3′
SM22α promoter Cre (forward)	5′-CCAGAGAACAGTGAAGTAGGAG-3′
SM22α promoter Cre (reverse)	5′-CATCCAGTCTTGCGAACCTCAT-3′
TIE2 promoter Cre (forward)	5′-CCCTGTGCTCAGACAGAAATGAGA-3′
TIE2 promoter Cre (reverse)	5′-CGCATAACCAGTGAAACAGCATTGC-3′

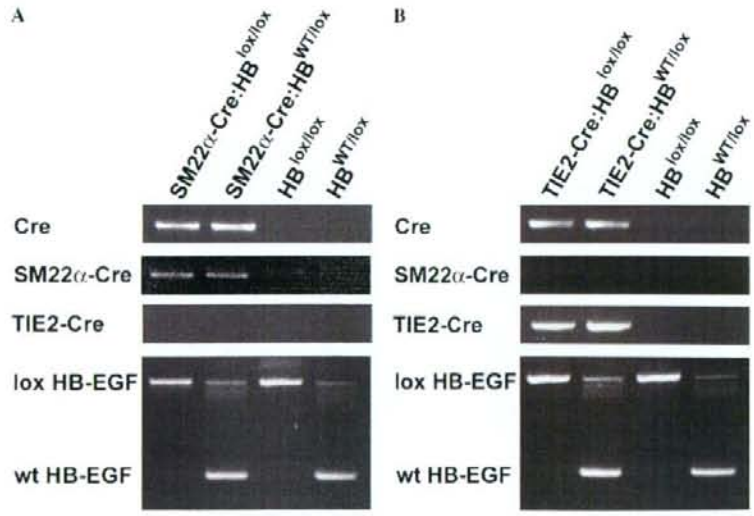

Fig. 1. Genotypes of the conditional knockout mice. SM22α-Cre:$HB^{lox/lox}$ (A) and TIE2-Cre:$HB^{lox/lox}$ (B) mice were confirmed by PCR. *SM22α*-Cre but not *TIE2*-Cre transgenes were detected with SM22α-Cre specific primers and vice versa. The *HB-EGF* gene flanked by *loxP* sites and the wild-type gene were also confirmed by PCR genotyping.

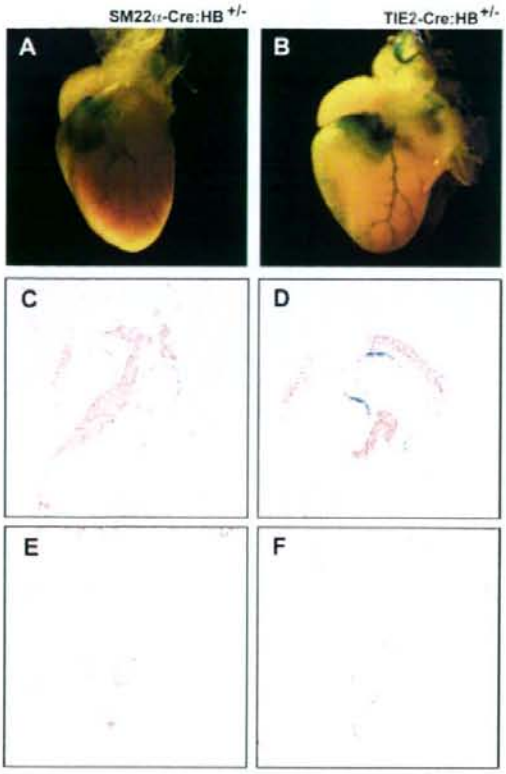

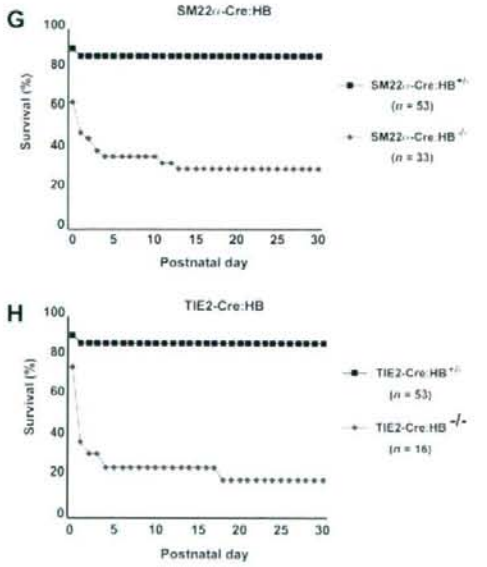

Histological analysis. Mouse tissues were fixed in 3.7% formaldehyde, dehydrated, and embedded in paraffin. Ten micrometer sections were stained with hematoxylin and eosin. For X-gal staining, after fixation with 2% formaldehyde and 0.2% glutaraldehyde, the tissues were stained with 5-bromo-4-chloro-3-indolyl β-D-galactoside (X-Gal). The stained tissues were fixed again with 3.7% formaldehyde, dehydrated, and embedded in paraffin. Ten micrometer sections were stained with eosin.

Results

Generation of HB-EGF conditional knockout mice

To generate cell-type specific HB-EGF knockout mice, mice carrying alleles with the *HB-EGF* gene flanked by *loxP* sites ($HB^{lox/lox}$; [6]) were crossed with SM22α-Cre [12] or TIE2-Cre [13] transgenic mice. The obtained mice carrying the wild-type and *loxP HB-EGF* genes, and Cre transgenes (SM22α-Cre:$HB^{WT/lox}$ or TIE2-Cre:$HB^{WT/lox}$, which we refer to as SM22α-Cre:$HB^{+/-}$ or TIE2-Cre:$HB^{+/-}$) were bred again with $HB^{lox/lox}$ mice to generate SM22α-Cre:$HB^{lox/lox}$ or TIE2-Cre:$HB^{lox/lox}$ mice, which we refer to as SM22α-Cre:$HB^{-/-}$ or TIE2-Cre:$HB^{-/-}$ mice. The genotype of mice was confirmed by PCR analysis (Fig. 1). No overt abnormalities were observed in $HB^{WT/lox}$ or $HB^{lox/lox}$ mice [6,23], and there was no evidence that strong expression of Cre recombinase induced abnormalities in wild-type mice.

HB-EGF expression in the heart of HB-EGF conditional knockout mice

The targeting vector used for the generation of $HB^{lox/lox}$ mice contains the *lacZ* reporter gene under the control of the native *HB-EGF* promoter, which is activated by Cre-mediated recombination [6]. Beta-gal staining of newborn (postnatal day 1; P1) hearts in SM22α-Cre:$HB^{+/-}$ and TIE2-Cre:$HB^{+/-}$ mice showed that HB-EGF was strongly expressed at the site where the great vessels and coronary arteries arise from the heart (Fig. 2A and B). Histological analysis of the heart revealed that β-gal positive cells were localized to the margins of all of the heart valves, including the semilunar (aortic and pulmonic) valves (Fig. 2C and D) and the atrioventricular (mitral and tricuspid) valves (Fig. 2E and F). These results indicate that HB-EGF expression was blocked in the endocardium of the heart valves and the coronary artery of SM22α-Cre:$HB^{-/-}$ and TIE2-Cre:$HB^{-/-}$ mice.

Fig. 2. The heart morphologies and the tissue sections of newborn (P1) SM22α-Cre:$HB^{+/-}$ and TIE2-Cre:$HB^{+/-}$ (corresponds to wild-type) mice and survival of conditional knockout mice. Whole mount β-gal staining revealed that HB-EGF was strongly expressed at sites at which the great vessels and coronary arteries arise from the heart in SM22α-Cre:$HB^{+/-}$ (A) and TIE2-Cre:$HB^{+/-}$ (B) mice. The longitudinal sections showed that HB-EGF was expressed at the margin of the semilunar (C; SM22α-Cre:$HB^{+/-}$ and D; TIE2-Cre:$HB^{+/-}$) and atrioventricular (E; SM22α-Cre:$HB^{+/-}$ and F; TIE2-Cre:$HB^{+/-}$) valves. Over half of the SM22α-Cre:$HB^{-/-}$ (G) and TIE2-Cre:$HB^{-/-}$ (H) mice died within the first day after birth. Approximately 70–80% of these knockout mice died with the first 2 weeks after birth.

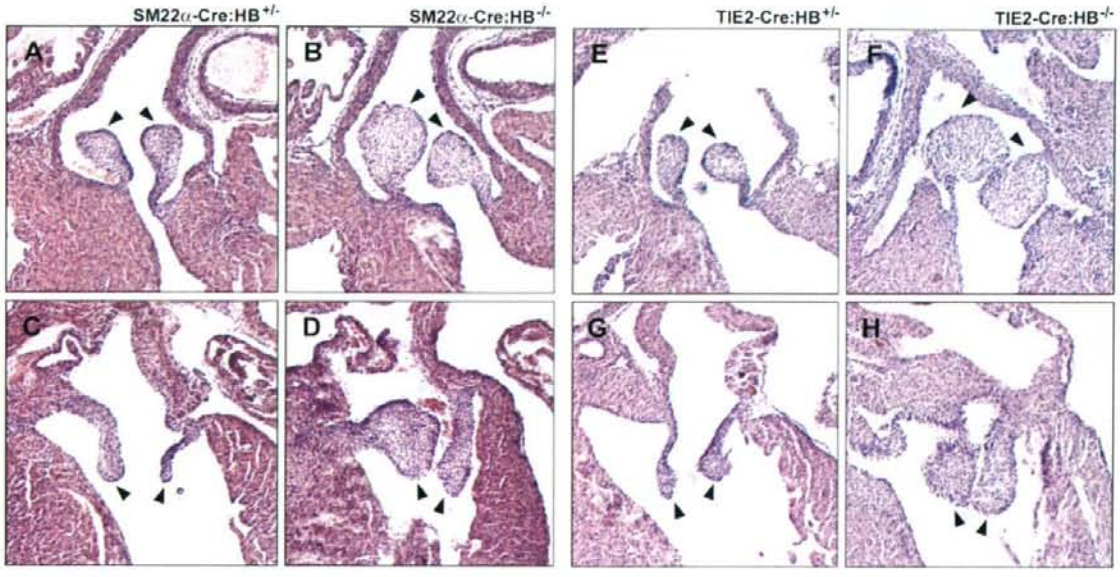

Fig. 3. Hematoxylin and eosin staining of the longitudinal sections of the newborn (P1) heart valves. Histological sections show semilunar (A, B, E and F) and atrioventricular (C, D, G and H) valves. In SM22α-Cre:$HB^{-/-}$ (B and D) and TIE2-Cre:$HB^{-/-}$ (F and H) mice, the valves were enlarged when compared with SM22α-Cre:$HB^{+/-}$ (A and C) and TIE2-Cre:$HB^{+/-}$ (E and G) mice. The valves are indicated with arrowheads.

Postnatal lethality of HB-EGF conditional knockout

Breeding of SM22α-Cre:$HB^{WT/lox}$ or TIE2-Cre:$HB^{WT/lox}$ with homozygous $HB^{lox/lox}$ mice yielded HB-EGF conditional knockout mice. Half of these mice died within one day after birth. Seventy percent of SM22α-Cre:$HB^{-/-}$ mice died within 13 days after birth (Fig. 2G), and 80% of TIE2-Cre:$HB^{-/-}$ mice died within 18 days after birth (Fig. 2H). SM22α-Cre:$HB^{-/-}$ and TIE2-Cre:$HB^{-/-}$ mice survivors displayed no obvious outward abnormalities and remained alive for at least several months after birth (data not shown).

Enlarged heart valves in HB-EGF conditional knockout mice

Histological analysis of newborn (P1) hearts revealed that SM22α-Cre:$HB^{-/-}$ and TIE2-Cre:$HB^{-/-}$ mice developed enlarged semilunar (Fig. 3A, B, E and F) and atrioventricular (Fig. 3C, D, G and H) valves when compared with SM22α-Cre:$HB^{+/-}$ and TIE2-Cre:$HB^{+/-}$ mice. This phenotype was consistent with that of HB-EGF-null mice [6,7]. The enlargement of neonatal heart in HB-EGF-deficient mice [6,7], however, was not observed in the P1 heart of these conditional knockout mice (data not shown).

Cardiac hypertrophy in HB-EGF conditional knockout mice

Although the survivors of SM22α-Cre:$HB^{-/-}$ and TIE2-Cre:$HB^{-/-}$ mice initially appeared normal, massive enlargement of the heart was apparent by 12 weeks of age when compared with control mice (Fig. 4A–D). Specifically, the mean heart-to-body wet weight ratio was $1.64 \pm 0.74\%$ for 12-week-old SM22α-Cre:$HB^{-/-}$ mice and was $0.65 \pm 0.16\%$ for 12-week-old SM22α-Cre:$HB^{+/-}$ mice (Fig. 4E). Further, the mean ratio of heart/body weight was $1.36 \pm 0.48\%$ for 12-week-old TIE2-Cre:$HB^{-/-}$ mice and was $0.76 \pm 0.063\%$ for 12-week-old TIE2-Cre:$HB^{+/-}$ mice (Fig. 4F).

Discussion

The present study demonstrated that loss of HB-EGF in smooth muscle or endothelial cell lineages resulted in heart valve malformations, postnatal lethality, and cardiac hypertrophy, which is a phenotype similar to that of HB-EGF-null mice [6,7]. The *HB-EGF* gene was deleted in endocardial cells of the heart valves in SM22α-Cre:$HB^{-/-}$ and TIE2-Cre:$HB^{-/-}$ mice. Data from the present study suggest that enlargement of the heart valves results from the loss of HB-EGF in the endocardial cells of heart valves, and the heart valve malformation is likely responsible for the postnatal lethality and cardiac hypertrophy of these *HB-EGF* conditional knockout mice.

Heart valves develop from endocardial cushions, which form when the endocardial cells undergo an endocardial-mesenchymal transition (EMT) and proliferate and invade the cardiac jelly, a basement membrane-like substance produced by the myocardial cells. The endocardial cushion area elongates and undergoes continuous remodeling to refine the primitive cushion into thin elongated valve leaflets.

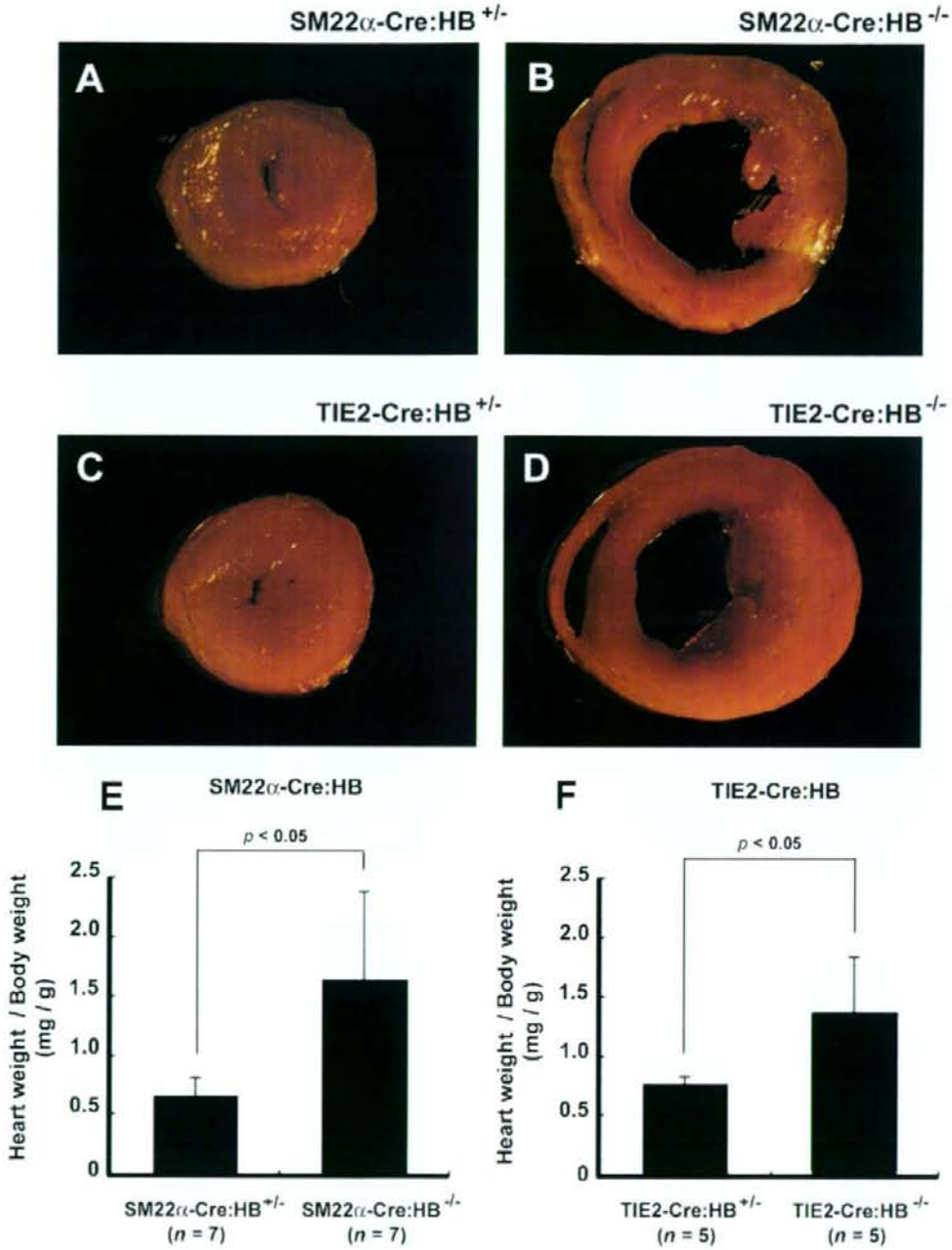

Fig. 4. Cardiac hypertrophy of the conditional knockout mice. Transverse sections of the hearts (A–D) and heart weight-to-body wet weight ratios (E and F) of 12-week-old mice. Values represent means ± SD. Massive enlargement of the heart was observed in SM22α-Cre:HB$^{-/-}$ and TIE2-Cre:HB$^{-/-}$ mice when compared with the control mice.

SM22α is expressed in cardiac muscle, smooth muscle, and skeletal muscle cells during embryogenesis, but becomes restricted to smooth muscle lineages at late embryonic stages and throughout adulthood [18]. Although HB-EGF is expressed in the heart [6,7], we could not detect obvious β-gal staining in myocardium of SM22α-Cre:HB$^{+/-}$ mice. *SM22α-lacZ* mice show the low expression of this transgene in myocardium during late development [24], which

suggests low *SM22α-Cre* activity and subsequent recombination efficiency with *loxP HB-EGF* in myocardium of SM22α-Cre:HB$^{+/-}$ mice. During early avian cardiac development, the endocardium-derived mesenchymal cells, which form endocardial cushions and subsequently form heart valves, have characteristics of smooth muscle-like myofibroblasts and express smooth muscle-specific alpha actin [25]. This finding suggests that the mesenchymal cells that had transformed from endocardial cells expressed the smooth muscle-specific *SM22α* gene, and this fact may account for *HB-EGF* gene deletion in the heart valves of SM22α-Cre:HB$^{-/-}$ mice.

TIE2 is expressed in endothelial cells throughout development [19,21,22]. Previous studies have reported that *TIE2*-Cre:R26R mice have β-galactosidase activity that was restricted to the endocardium and the mesenchyme of the endocardial cushions but was never observed in myocardium or epicardium of the developing heart [26]. These data indicate that the *HB-EGF* gene was eliminated in endocardial but not in myocardial cell lineages in the developing heart of TIE2-Cre:HB$^{-/-}$ mice. Therefore, the present study suggests that the loss of endocardial but not myocardial HB-EGF is at least responsible for the heart valve enlargement in HB-EGF-null mice.

Enlargement of heart valves has also been observed in mutant mice expressing an uncleavable form of proHB-EGF [27], in ADAM17-null mice [7], in EGFR-null mice with a CD1 background, and in mice expressing a mutant EGFR (*waved-2*) [8]. Together with data from the present study, these observations indicate that ectodomain shedding of proHB-EGF in endocardial cells of heart valves and subsequent EGFR activation are essential for remodeling of endocardial cushions. Although the mechanism of cushion remodeling is largely unknown, HB-EGF/EGFR signaling in the mesenchymal cells within the endocardial cushions may suppress cellular proliferation to refine the primitive cushion into thin elongated valve leaflets [7,28]. Recent studies have reported that the cytoplasmic domain of proHB-EGF and C-terminal fragment of proHB-EGF generated by ectodomain shedding have some functions [29–31]. These intracellular signaling might be involved in the heart valve formation.

In conclusion, the loss of *HB-EGF* gene expression in smooth muscle or endothelial cell lineages of the developing mouse results in heart valve malformations and cardiac hypertrophy. These data indicate the significance of endocardial HB-EGF for proper heart development and function.

Acknowledgments

This work is supported by Grants-in-Aid for Scientific Research (No. 17390081) to S.H. from the Ministry of Education, Culture, Sports, Science and Technology of Japan, and Precursory Research for Embryonic Science and Technology (Information and Cell Function).

References

[1] S. Higashiyama, J.A. Abraham, J. Miller, J.C. Fiddes, M. Klagsbrun, A heparin-binding growth factor secreted by macrophage-like cells that is related to EGF, Science 251 (1991) 936–939.
[2] S. Higashiyama, K. Lau, G. Besner, J.A. Abraham, M. Klagsbrun, Structure of heparin-binding EGF-like growth factor: multiple forms, primary structure, and glycosilation of the mature protein, J. Biol. Chem. 267 (1992) 6205–6212.
[3] R. Iwamoto, E. Mekada, Heparin-binding EGF-like growth factor: a juxtacrine growth factor, Cytokine Growth Factor Rev. 11 (2000) 335–344.
[4] E. Nishi, M. Klagsbrun, Heparin-binding epidermal growth factor-like (HB-EGF) is a mediator of multiple physiological and pathological pathways, Growth factors 22 (2004) 253–260.
[5] S. Higashiyama, D. Nanba, ADAM-mediated ectodomain shedding of HB-EGF in receptor cross-talk, Biochim. Biophys. Acta. 1751 (2005) 110–117.
[6] R. Iwamoto, S. Yamazaki, M. Asakura, S. Takashima, H. Hasuwa, K. Miyado, S. Adachi, M. Kitakaze, K. Hashimoto, G. Raab, D. Nanba, S. Higashiyama, M. Hori, M. Klagsbrun, E. Mekada, Heparin-binding EGF-like growth factor and ErbB signaling is essential for heart function, Proc. Natl. Acad. Sci. USA 100 (2003) 3221–3226.
[7] L.F. Jackson, T.H. Qiu, S.W. Sunnarborg, A. Chang, C. Zhang, S. Patterson, D.C. Lee, Defective valvulogenesis in HB-EGF and TACE-null mice is associated with aberrant BMP signaling, EMBO J. 22 (2003) 2704–2716.
[8] B. Chen, R.T. Bronson, L.D. Klaman, T.G. Hampton, J.F. Wang, P.J. Green, T. Magnouson, P.S. Douglas, J.P. Morgan, B.G. Neel, Mice mutant for Egfr and Shp2 have defective cardiac semilunar valvulogenesis, Nat. Genet. 24 (2000) 96–299.
[9] S.W. Sunnarborg, C.L. Hinkle, M. Stevenson, W.E. Russell, C.S. Raska, J.J. Peschon, B.J. Castner, M.J. Gerhart, R.J. Paxton, R.A. Black, D.C. Lee, Tumor necrosis factor-alpha converting enzyme (TACE) regulates epidermal growth factor receptor ligand availability, J. Biol. Chem. 277 (2002) 12838–12845.
[10] U. Sahin, G. Weskamp, K. Kelly, H. Zhou, S. Higashiyama, J. Peschon, D. Hartmann, P. Saftig, C.P. Blobel, Distinct roles for ADAM10 an ADAM17 in ectodomain shedding of six EGFR ligands, J. Cell Biol. 164 (2004) 769–779.
[11] M. Asakura, M. Kitakaze, S. Takashima, Y. Liao, F. Ishikura, T. Yoshinaka, H. Ohmoto, K. Node, K. Yoshino, H. Ishiguro, H. Asanuma, S. Sanada, Y. Matsumura, H. Takeda, S. Beppu, M. Tada, M. Hori, S. Higashiyama, Cardiac hypertrophy is inhibited by antagonism of ADAM12 processing of HB-EGF: metalloproteinase inhibitors as a new therapy, Nature Med. 8 (2002) 35–40.
[12] R. Holtwick, M. Gotthardt, B. Skryabin, M. Steinmetz, R. Potthast, B. Zetsche, R.E. Hammer, J. Herz, M. Kuhn, Smooth muscle-selective deletion of guanylyl cyclase-A prevents the acute but not chronic effects of ANP on blood pressure, Proc. Natl. Acad. Sci. USA 99 (2002) 7142–7147.
[13] P.A. Koni, S.K. Joshi, U.A. Temann, D. Olson, L. Burkly, R.A. Flavell, Conditional vascular cell adhesion molecule 1 deletion in mice: impaired lymphocyte migration to bone marrow, J. Exp. Med. 193 (2001) 741–754.
[14] J.P. Lee-Miller, D.H. Heeley, L.B. Smillie, An abundant and novel protein of 22 kDa (SM22) is widely distributed in smooth muscles: purification from bovine aorta, Biochem. J. 244 (1987) 705–709.
[15] S.J. Winder, C. Sutherland, M.P. Walsh, Biochemical and functional characterization of smooth muscle calponin, Adv. Exp. Med. Biol. 304 (1991) 37–51.
[16] J.L. Duband, M. Gimona, M. Scatena, S. Sartore, J.V. Small, Calponin and SM 22 as differentiation markers of smooth muscle: spatiotemporal distribution during avian embryonic development, Differentiation 55 (1993) 1–11.

[17] W. Nishida, Y. Kitami, K. Hiwada, cDNA cloning and mRNA expression of calponin and SM22 in rat aorta smooth muscle cells, Gene 130 (1993) 297–302.
[18] L. Li, J.M. Miano, P. Cserjesi, E.N. Olson, SM22α, a marker of adult smooth muscle, is expressed in multiple myogenic lineages during embryogenesis, Circ. Res. 78 (1996) 188–195.
[19] T.N. Sato, Y. Qin, C.A. Kozak, K.L. Audus, Tie-1 and tie-2 define another class of putative receptor tyrosine kinase genes expressed in early embryonic vascular system, Proc. Natl. Acad. Sci. USA 90 (1993) 9355–9358.
[20] S. Davis, T.H. Aldrich, P.F. Jones, A. Acheson, D.L. Compton, V. Jain, T.E. Ryan, J. Bruno, C. Radziejewski, P.C. Maisonpierre, G.D. Yancopoulous, Isolation of angiopoietin-1, a ligand for the TIE2 receptor, by secretion-trap expressing cloning, Cell 87 (1996) 1161–1169.
[21] H. Schnürch, W. Risau, Expression of tie-2, a member of a novel family of receptor tyrosine kinases, in the endothelial cell lineage, Development 119 (1993) 957–968.
[22] A.L. Wong, Z.A. Haroon, S. Werner, M.W. Dewhirst, C.S. Greenberg, K.G. Peters, Tie2 expression and phosphorylation in angiogenic and quiescent adult tissues, Circ. Res. 81 (1997) 567–574.
[23] Y. Shirakata, R. Kimura, D. Nanba, R. Iwamoto, S. Tokumaru, C. Morimoto, K. Yokota, M. Nakamura, K. Sayama, E. Mekada, S. Higashiyama, K. Hashimoto, Heparin-binding EGF-like growth factor accelerates keratinocyte migration and skin wound healing, J. Cell Sci. 118 (2005) 2363–2370.
[24] L. Li, J.M. Miano, M. Mercer, E.N. Olson, Expression of the *SM22α* promoter in transgenic mice provides evidence for distinct transcriptional regulatory programs in vascular and visceral smooth muscle cells, J. Cell Biol. 132 (1996) 849–859.
[25] Y. Nakajima, V. Mironov, T. Yamagishi, H. Nakamura, R.R. Markwald, Expression of smooth muscle alpha-actin in mesenchymal cells during formation of avian endocardial cushion tissue: a role for transforming growth factor β3, Dev. Dyn. 209 (1997) 296–309.
[26] F.J. de Lange, A.F.M. Moorman, R.H. Anderson, J. Männer, A.T. Soufan, C. de Gier-de Vries, M.D. Schneider, S. Webb, M.J.B. van den Hoff, V.M. Christoffels, Lineage and morphogenetic analysis of the cardiac valves, Cir. Res. 95 (2004) 645–654.
[27] S. Yamazaki, R. Iwamoto, K. Saeki, M. Asakura, S. Takashima, A. Yamazaki, R. Kimura, H. Mizushima, H. Moribe, S. Higashiyama, M. Endoh, Y. Kaneda, S. Takagi, S. Itami, N. Takeda, G. Yamada, E. Mekada, Mice with defects in HB-EGF ectodomain shedding show severe developmental abnormarities, J. Cell Biol. 163 (2003) 469–475.
[28] R. Iwamoto, E. Mekada, ErbB and HB-EGF signaling in heart development and function, Cell Struct. Funct. 31 (2006) 1–14.
[29] J. Lin, L. Hutchinson, S.M. Gaston, G. Raab, M.R. Freeman, BAG-1 is a novel cytoplasmic binding partner of the membrane form of heparin-binding EGF-like growth factor: a unique role for proHB-EGF in cell survival regulation, J. Biol. Chem. 276 (2001) 30127–30132.
[30] D. Nanba, A. Mammoto, K. Hashimoto, S. Higashiyama, Proteolytic release of the carboxy-terminal fragment of proHB-EGF causes nuclear export of PLZF, J. Cell Biol. 163 (2003) 489–502.
[31] X. Wang, H. Mizushima, S. Adachi, M. Ohishi, R. Iwamoto, E. Makada, Cytoplasmic domain phosphorylation of heparin-binding EGF-likegrowth factor, Cell Struct. Funct. 31 (2006) 15–27.

Journal of General Virology (2007), **88**, 2463–2472 DOI 10.1099/vir.0.82881-0

A comprehensive library of mutations of Epstein–Barr virus

Ya-Fang Chiu,[1] Chao-Ping Tung,[1] Yu-Hisu Lee,[1] Wen-Hung Wang,[1] Ching Li,[2] Jia-Yan Hung,[3] Chen-Yu Wang,[1] Yasushi Kawaguchi[4] and Shih-Tung Liu[1]

Correspondence
Shih-Tung Liu
cgliu@mail.cgu.edu.tw

[1]Molecular Genetics Laboratory, Department of Microbiology and Immunology, Chang Gung University, Taoyuan 333, Taiwan

[2]Department of Applied Microbiology, National Chiayi University, Chiayi City 600, Taiwan

[3]Institute of Biochemistry and Biotechnology, Chung Shan Medical University, Taichung 402, Taiwan

[4]Division of Viral Infection, Department of Infectious Disease Control, International Research Center for Infections Diseases, The Institute of Medical Science, The University of Tokyo, 4–6–1 Shirokanedai, Minato-Ku, Tokyo 108–8639, Japan

Received 25 January 2007
Accepted 14 May 2007

A mutant library of 249 mutants with mutations that span the entire Epstein–Barr virus (EBV) genome was generated by transposition with EZ::TN <KAN-2> and insertion with an apramycin resistance gene by a PCR-targeting method. This study also demonstrates the feasibility of generating deletions and site-specific mutations in the *BRLF1* promoter on the EBV genome to determine the regions in the promoter that are crucial to transcription. Analysing *BZLF1* and *BRLF1* mutants by microarray analysis revealed that these two genes regulate the transcription of EBV lytic genes differently. A *BZLF1* mutation affects global expression of EBV lytic genes; almost no lytic gene is expressed by the mutant after lytic induction. However, although a *BRLF1* mutant still transcribes most lytic genes, the expression of these lytic genes is inefficient. Furthermore, this study shows that the proximal Zta-response element in the *BRLF1* promoter is crucial to *BRLF1* transcription from the EBV genome, despite the fact that another work demonstrated that this site was unimportant in transient transfection analysis. Furthermore, mutants with a mutation in *BDLF1* and *BORF1* cannot assemble viral capsids. Results of this study demonstrate the usefulness of a comprehensive mutant library in genetic analyses of EBV.

INTRODUCTION

Mutational analyses underlie genetic investigations. These analyses are particularly powerful for a virus with a large genome, such as the Epstein–Barr virus (EBV). Although only a few EBV mutants have been available for study in the past, they have nonetheless yielded valuable information on the function of EBV genes. Many of these mutants have arisen spontaneously. For instance, *BYRF1* and *BALF2*, which encode EBNA2 (Epstein–Barr virus nuclear antigen 2) and the ssDNA-binding protein, are deleted in strains P3HR1 and Raji, respectively. Work on these strains demonstrated the involvement of these genes in regulating the expression of latent membrane protein 1 (LMP1) and lytic DNA replication (Decaussin *et al.*, 1995; Hatfull *et al.*, 1988; Skare *et al.*, 1985). EBV mutants can also be generated by inserting a drug-resistance gene at a specific target site by recombination in a cell line. For instance, a mutation in *BZLF2*, which encodes gp42, was generated by this approach. Analysis of the mutant revealed that gp42 is critical in the fusion of EBV to the host plasma membrane, and so affects the tropism and infectivity of EBV (Wang & Hutt-Fletcher, 1998). Another approach to generate EBV mutants involves a strain generated in the laboratory, called maxi-EBV (Delecluse *et al.*, 1998). This EBV strain is obtained by inserting an F replicon into the EBV genome by recombination; this insertion influences neither the latent nor the lytic functions of the virus. Therefore, the EBV strain can be maintained and its genes can then be mutated by *recA*-dependent homologous recombination in *Escherichia coli*. Following mutagenesis, the mutant EBV is studied in B lymphocytes or 293 cells. Many mutants have been generated in this way and the impact of the mutations on EBV's life cycle and its host cell has been elucidated (Altmann *et al.*, 2006; Chau *et al.*, 2006; Chen *et al.*, 2005; Collins *et al.*, 2002; Delecluse *et al.*, 1999; Dirmeier *et al.*, 2003; Farina *et al.*, 2005; Feederle & Delecluse, 2004;

Supplementary material and sequences of the primers used are available with the online version of this paper.

Feederle *et al.*, 2000, 2005, 2006; Grabusic *et al.*, 2006; Hong *et al.*, 2004; Humme *et al.*, 2003; Hutchings *et al.*, 2006; Janz *et al.*, 2000; Kelly *et al.*, 2005; Neuhierl & Delecluse, 2006). Feederle *et al.* (2000) examined a mutant that contained a mutated *BRLF1* and demonstrated that the protein encoded by this gene, Rta, is critical to the expression of EBV late proteins, including gp110, VCA (viral capsid antigen) and gp350/220. Additionally, the mutant strain does not yield EBV particles (Feederle *et al.*, 2000), revealing the importance of Rta in the lytic development of EBV. The same work also demonstrated that a mutant strain with a defective *BZLF1*, which encodes Zta, does not yield infectious EBV particles following lytic induction by Rta (Feederle *et al.*, 2000), indicating that Zta is critical to the lytic development of EBV. A study of a mutation in *BLLF1*, which encodes gp350/220, demonstrated that the EBV infection of B lymphocytes may not depend on the binding of gp350/220 to CD21 (Janz *et al.*, 2000). A mutation in *BNLF1*, which encodes LMP1, was found to influence the production of EBV (Ahsan *et al.*, 2005; Kanda *et al.*, 2004). A similar mutagenesis study also demonstrated the importance of Zta and the Zta-response element (ZRE) in the *oriLyt* in EBV lytic DNA replication (Feederle & Delecluse, 2004). A recent study showed that a mutation in *BMRF1* affects EBV lytic DNA replication and lytic development (Neuhierl & Delecluse, 2006). A mutation in *BLLF1* also allows EBV to infect epithelial cells (Shannon-Lowe *et al.*, 2006). One limitation in the mutagenesis employed in these studies is that it is targeted to specific genes. Recently, a new method that uses bacterial transposons has been used to generate random insertions in the genome of Kaposi's sarcoma-associated herpesvirus (KHSV) and murine gammaherpesvirus 68 (Song *et al.*, 2005). Here, we have adopted two mutagenesis methods and established a comprehensive library of EBV mutants, which is useful in the genetic analysis of EBV.

METHODS

Bacterial strains, plasmids, transposon, EBV and cell lines. 293 is a human embryonic epithelial kidney cell line. 293-B95-8/F is a 293 cell line that contains maxi-EBV (Delecluse *et al.*, 1998). 293, 293-B95-8/F cells and 293 cells that contained mutant EBV strains were cultured in Dulbecco's modified Eagle's medium that contained 10 % fetal calf serum. *E. coli* EPI300 and transposon EZ::TN <KAN-2> were purchased from Epicentre. Plasmids pCMV-R and pCMV-Z were used to express Rta and Zta, respectively (Chang & Liu, 2000; Hung & Liu, 1999). *BORF1* was amplified by PCR, using BORF1-F (5′-CGCGGATCCGACGCCATGAAGGTCCAG-3′) and BORF1-R (5′-GGCCTCGAGCCTCCTCCTCCTGTTTCC-3′) as primers, and EBV DNA as a template. The fragment was inserted into the *Bam*HI and *Xho*I sites of pcDNA3-HA to generate plasmid pHA-BORF1. Plasmid pHA-BDLF1 was obtained by inserting a *BDLF1* fragment that was amplified with primers BDLF1-F (5′-CCGGAATTCA-TGGATTTGAAAGTGGTA-3′) and BDLF1-R (5′-CCGCTCG-AGTTATCTTAACCAGCAAGT-3′) into the *Eco*RI and *Xho*I sites of pcDNA3-HA. *E. coli* BW25113 is a host used for PCR targeting (Datsenko & Wanner, 2000; Gust *et al.*, 2003). Plasmid pKD46 is temperature-sensitive and carried λ-RED recombinase genes that could be induced by culturing the bacteria in an arabinose-containing medium (Datsenko & Wanner, 2000; Gust *et al.*, 2003). Plasmid pIJ773 (Datsenko & Wanner, 2000; Gust *et al.*, 2003) was used as a template for amplifying an apramycin-resistance cassette for PCR targeting.

Isolating maxi-EBV DNA. Maxi-EBV was isolated from 293-B95-8/F cells using an alkaline-lysis method (Griffin *et al.*, 1981) and transformed into *E. coli* EPI300 by electroporation (Sharma & Schimke, 1996). Transformants were selected on Luria–Bertani (LB) agar that contained 20 μg chloramphenicol ml^{-1}. The presence of maxi-EBV DNA in *E. coli* was examined by the alkaline-lysis method of Kado & Liu (1981).

Purifying EBV DNA from *E. coli*. Maxi-EBV and EBV mutant DNA were purified from *E. coli* EPI300 with a Midi plasmid purification kit (Qiagen) according to the manufacturer's protocol, except in that 20 ml each of P1, P2 and P3 buffer was used.

Transposition. Maxi-EBV (1 μg) was incubated with 7 ng EZ::TN <KAN-2> and 1 U Tn5 transposase in transposition buffer (Epicentre) for 2 h at 37 °C. One-tenth of the DNA in the mixture was employed to transform *E. coli* EPI300 by electroporation. Transformants were selected on LB agar that contained 50 μg kanamycin ml^{-1} and 20 μg chloramphenicol ml^{-1}.

Mutating the EBV genome by PCR targeting. A PCR-targeting method (Datsenko & Wanner, 2000; Gust *et al.*, 2003) was employed to insert an apramycin-resistance cassette into the maxi-EBV genome in *E. coli* BW25113. To accomplish this, a DNA fragment that contained an apramycin cassette was amplified by PCR, using pIJ773 (Datsenko & Wanner, 2000; Gust *et al.*, 2003) as a template. The primers used in PCR included a sequence in the 3′ region that complements the end of the cassette and a 39 bp sequence in the 5′ region that complements the EBV target sequences (Supplementary Table S3). An amplified fragment was transformed by electroporation into *E. coli* BW25113(pKD46, maxi-EBV) that was pre-cultured at 30 °C in LB broth containing 0.2 % arabinose (Datsenko & Wanner, 2000; Gust *et al.*, 2003). Subsequently, pKD46 was cured by culturing the cells at 37 °C on LB agar. *E. coli* that contained mutated maxi-EBV was selected on LB agar that contained 50 μg apramycin ml^{-1} and 20 μg chloramphenicol ml^{-1}. To mutate the three ZREs in the *BRLF1* promoter in the EBV genome, an apramycin resistance gene that was amplified by PCR, using pIJ773 as a template, was inserted into the *Dra*I site located at position −965 of the *BRLF1* promoter in pRp (Chang & Liu, 2000). The three ZREs in the promoter at −251, −191 and −34 in the plasmid were subsequently mutated from 5′-TTCGCGA-3′ to 5′-GAATTCA-3′, 5′-TGAGCGA-3′ to 5′-TGGATCC-3′ and 5′-TGAGCCAT-3′ to 5′-TGGATATC-3′, respectively, by site-directed mutagenesis (Ho *et al.*, 1989). DNA fragments that contained the apramycin resistance gene and the entire *BRLF1* promoter were amplified from the plasmids with primers GL2-R/Apr-F and GL2-R/Apr-R (Supplementary Table S3). The fragments were finally used to replace the *BRLF1* promoter on the EBV genome by PCR targeting.

DNA sequencing. Mutations of the EBV genome were confirmed by DNA sequencing with a SequiTherm EXCEL II DNA sequencing kit-LC (Epicentre) and an automated DNA sequencer (model 4000L; LI-COR).

Transfection and selection. Approximately 9×10^5 293 cells were transfected with 2 μg EBV DNA with Lipofectamine 2000, according to the method recommended by the manufacturer (Invitrogen). Following transfection, cells were selected with a medium containing 200 μg hygromycin ml^{-1} (Invitrogen) for

3 weeks. Transfection of plasmids was performed with a Bio-Rad Gene Pulser electroporator.

Immunoblot analysis. Proteins from 1×10^7 cells lytically induced for 24 h with 12-O-tetradecanoylphorbol-13-acetate (TPA; 30 ng ml^{-1}) and 3 mM sodium butyrate were extracted with 0.5 ml lysis buffer (63 mM Tris/HCl, pH 6.8, 2 % SDS, 0.0025 % bromophenol blue, 10 % glycerol and 50 mM DTT). EBV virions were collected by ultracentrifugation 5 days after lytic induction of 1×10^8 cells. The pellet was suspended in 100 µl TNE buffer (0.01 M Tris/HCl, pH 7.5, 0.15 M NaCl and 1 mM EDTA) and an electrophoresis sample buffer (Sambrook *et al.*, 1989) was added to extract viral capsid proteins. Following extraction, proteins were separated by SDS-PAGE (Sambrook *et al.*, 1989) and transferred onto Immobilon-P membrane (Millipore). Antibodies against Rta and α-tubulin were purchased from Argene and Sigma, respectively. Anti-BORF1, anti-BDLF1 and anti-BcLF1 antibodies were generated in rabbit. Anti-EBNA1 antibody was obtained from Mei Chao (Chang Gung University, Taiwan). Protein bands were visualized using SuperSignal West Pico Chemiluminescent substrate (Pierce).

Microarray analysis of the transcription of EBV genes. The transcription of EBV genes was analysed by hybridization with an EBV DNA chip of 4.2×2.4 mm according to a method described elsewhere (Chang *et al.*, 2003; Li *et al.*, 2006). Total mRNA was purified from the cells using an Oligotex mRNA isolation kit (Qiagen). A cDNA hybridization probe was prepared by reverse transcription and hybridization was performed according to a method described elsewhere (Chang *et al.*, 2003; Li *et al.*, 2006).

Isolation of EBV particles, sucrose-gradient sedimentation analysis and real-time PCR. Cells (4×10^6) that contained maxi-EBV or its mutants were treated with 3 mM sodium butyrate and 30 ng TPA ml^{-1} to induce the EBV lytic cycle. After 5 days of culturing, cell debris in the culture medium was removed by centrifugation at 600 ***g*** for 7 min. The supernatant was then filtered through a 0.45 µm filter. EBV particles in the filtrate were pelleted by centrifugation at 25 000 ***g*** for 2 h. The pellet was suspended in 0.2 ml TNE buffer and subsequently treated with proteinase K and DNase I according to a method described elsewhere (Bloss & Sugden, 1994). In sucrose-gradient sedimentation analysis, the virus particle collected from the culture medium by ultracentrifugation was loaded onto a 20–60 % sucrose gradient that was prepared with a Gradient Station (Biocomp Instruments). To analyse the EBV capsids inside the cell, cells were lysed using a freeze-and-thaw procedure, which involved freeze-and-thaw four times for 3 min in liquid nitrogen and 3 min at 37 °C. The lysate was then subjected to sucrose-gradient centrifugation analysis. The gradient was centrifuged using a Beckman SW41Ti rotor at 25 000 ***g*** and 4 °C for 2 h. EBV DNA in each fraction was extracted following a method described elsewhere (Wang *et al.*, 2005). The amount of EBV genome was determined by real-time PCR using an iCycler iQ multicolor real-time PCR detection system (Bio-Rad) with primers and a probe that were specific to the *BKRF1* region (Ryan *et al.*, 2004).

RNA analysis. RNA was isolated from cells with TRIzol (Invitrogen) according to the method suggested by the manufacturer. Reverse transcription was performed with random hexamers and M-MLV reverse transcriptase (Promega). Real-time PCR was performed using two *BRLF1* primers, 5′- GAAGCCCGGTGCC-CAAAG-3′ and 5′-GTGTCACTGTTGCCCGAGTC-3′. The probe sequence for the amplified *BRLF1* region was 5′-(6FAM)CGGTG-ACAGCAGTTCCAGCAGCA (TAMRA)-3′. A fragment was also amplified from *BKRF1* and quantified by real-time PCR (Ryan *et al.*, 2004), which was used as a control to normalize the amplification results.

RESULTS

Generating EBV mutants with EZ::TN <KAN-2>

Maxi-EBV DNA was mutated with EZ::TN <KAN-2> *in vitro*. After transposition, one-tenth of the reaction, which contained 0.1 µg maxi-EBV DNA, was transformed into *E. coli* EPI300. Maxi-EBV that contained an EZ::TN <KAN-2> insertion was selected by plating the transformants on LB agar that contained chloramphenicol and kanamycin. The transformation yielded around 5000 drug-resistant colonies. Screening 100 colonies by the alkaline-lysis method of Kado & Liu (1981) revealed the presence of a plasmid of about 170 kb, which was consistent with the size of maxi-EBV DNA. Insertion of the transposon into the genome in these EBV mutants was verified by Southern blotting with an EZ::TN <KAN-2> probe (data not shown) and DNA sequencing. The integrity of the DNA from 210 mutants, which contained a single transposon insertion, was confirmed by *Bam*HI and *Xho*I digestion (data not shown). Forty-four mutants with a transposon inserted in the terminal repeats, W-repeats and *oriLyt* repeats were also isolated. Analysis of these mutants demonstrated that 60 of the 93 annotated EBV genes were mutated (Fig. 1; Supplementary Table S1).

Mutating EBV genes by PCR targeting

Although transposon insertion yielded 60 mutants, screening for mutants that contain a mutation in the remaining 33 genes on the EBV genome from a large pool of mutants can be difficult. Therefore, a PCR-targeting method (Datsenko & Wanner, 2000; Gust *et al.*, 2003) was utilized to insert an apramycin resistance gene into a specific site on the EBV genome to complete a comprehensive mutant library. Accordingly, 39 additional mutants were generated (Fig. 1; Supplementary Table S1). Furthermore, DNA from the mutants was digested using *Bam*HI, *Xho*I and *Kpn*I; the restriction profiles were compared with those from maxi-EBV to determine the integrity of the DNA.

Transcription of EBV genes by *BRLF1* and *BZLF1* mutants

Analysis of two mutant strains, MI-270 and D-26, that contained mutated *BRLF1* and *BZLF1*, respectively, revealed that the mutations affected the expression of Rta, Zta, EA-D, gp350/220 and the production of EBV particles (Supplementary Fig. S1). Furthermore, the functions of these two genes could be genetically complemented by transfecting plasmids that expressed Rta and Zta (Supplementary Fig. S1). To further investigate how these two mutations influenced the overall transcription of EBV genes, a microarray study was subsequently performed with an EBV microarray chip. For hybridization, mRNA purified from cells was reverse transcribed, labelled with biotin and used as a probe. The hybridization results indicated that lytic genes were not expressed or

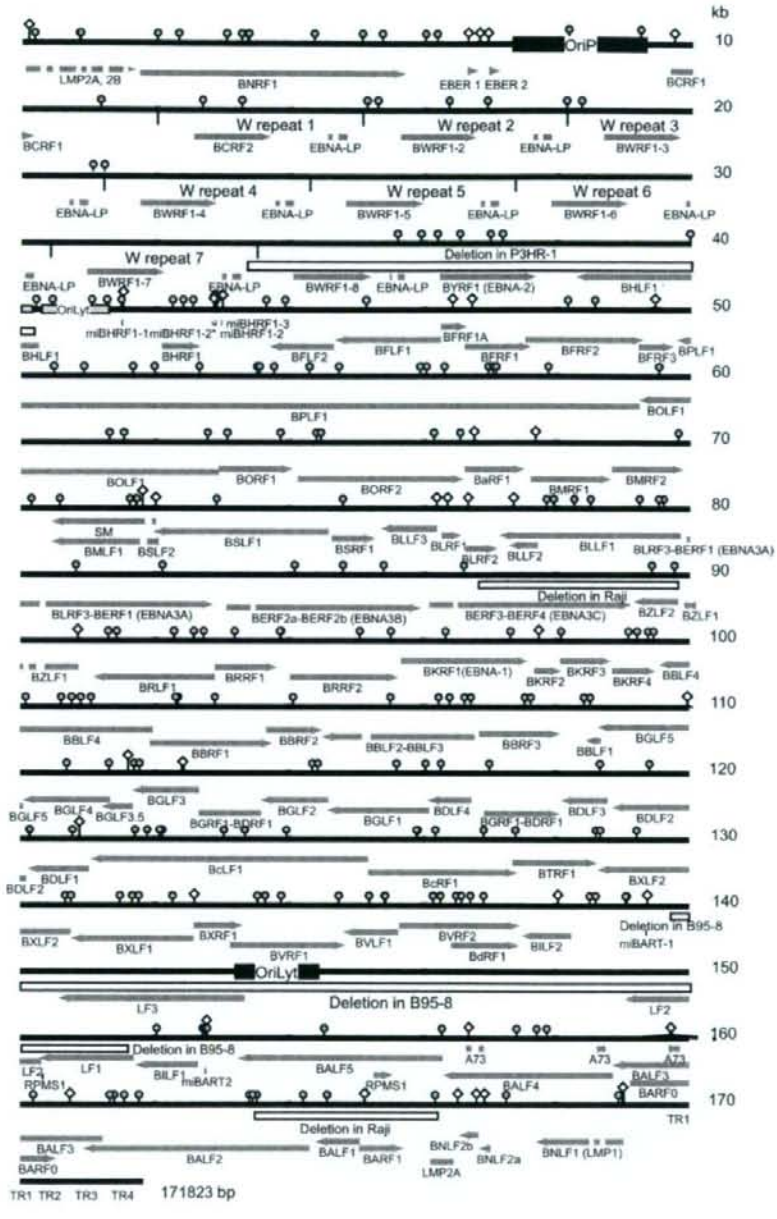

Fig. 1. Location of EZ::TN <KAN-2> and the apramycin-resistance cassette insertions in the EBV genome (GenBank accession no. AJ507799). ○: EZ::TN <KAN-2> insertion; ◇, apramycin-resistance cassette insertion; grey arrow, EBV genes; white box, deletion in different EBV strains; TR1–TR4, terminal repeats.

expressed at low levels by maxi-EBV during latency (Fig. 2a; Supplementary Table S2). Expression of EBV lytic genes was significantly enhanced after lytic induction with TPA and sodium butyrate (Fig. 2d; Supplementary Table S2). In the case of a *BZLF1* mutant, D-26, almost no lytic genes were expressed after TPA and sodium butyrate treatment (Fig. 2e; Supplementary Table S2). Meanwhile, transfecting pCMV-Z restored the expression of these lytic genes

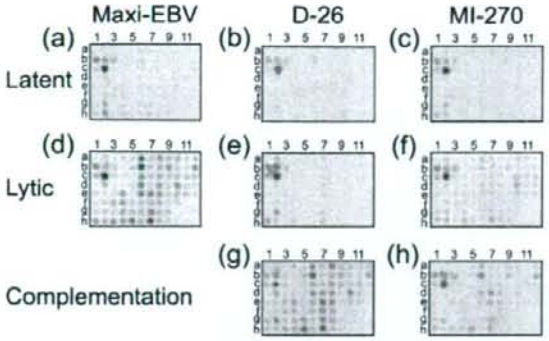

Fig. 2. Analysis of the transcription of EBV genes. mRNA was prepared from 293 cells that contained maxi-EBV (a, d), a *BZLF1* mutant (D-26) (b, e, g) and a *BRLF1* mutant (MI-270) (c, f, h) after the cells were treated with TPA and sodium butyrate (d–f), transfected with pCMV-Z (g) or pCMV-R (h) for 24 h. Control dots are in the upper-right-hand corner between columns 1 and 4 and rows a and d. Spot 1b contains a DNA fragment from a plant gene, *GA4*; during hybridization, a biotin-labelled probe that is specific for this spot was added and used as an external control to monitor the hybridization process. Spot 2c contains a DNA fragment from a plant gene, *rca*. The mRNA of *rca* was added during reverse transcription and used to monitor reverse transcription. Spot 2b contained a *GAPDH* fragment and was used as an internal control. Supplementary Table S2 states the EBV genes that are contained by each spot.

(Fig. 2g; Supplementary Table S2). Unlike mutant D-26, mutant MI-270 expressed most of the lytic genes after lytic induction, but at reduced levels (Fig. 2f; Supplementary Table S2). The expression was elevated after pCMV-R was transfected (Fig. 2h; Supplementary Table S2).

Effect of mutations in the *BRLF1* promoter on the transcription of *BRLF1*, expression of Rta and production of EBV particles

Functions of an EBV promoter were frequently studied by using a transient transfection assay. However, the assay system, although useful, may have its limitations and may not truly reflect how a gene is transcribed from the EBV genome, because the chromatin structure and copy number of the promoter in a reporter plasmid that is analysed in transient transfection assays may differ considerably from those on the EBV genome. The *BRLF1* promoter (Rp) is known to contain three ZREs. Earlier transient transfection studies yielded conflicting results on the function of one of these elements, ZRE1 (Fig. 3a). Although Sinclair *et al.* (1991) demonstrated the importance of ZRE1 in the transcription of *BRLF1*, Bhende *et al.* (2004) showed that this site was unimportant. Therefore, in this study we deleted Rp and also mutated the three ZREs in Rp on the EBV genome (Fig. 3a) to examine how these mutations affected *BRLF1* transcription. Meanwhile, an EBV strain with an inserted apramycin-resistance gene at position −965 in Rp (EB-Apr) (Fig. 3a) was used as a control. A separate set of mutants was also generated in independent experiments to confirm the reproducibility of the results. Real-time PCR revealed that inserting an apramycin-resistance gene at position −965 (EB-Apr) did not influence the transcription of *BRLF1*; the amount of *BRLF1* mRNA expressed by EB-Apr was about equal to that exhibited by maxi-EBV (Fig. 3). Deleting the region between positions −965 and −852 in the *BRLF1* promoter (Fig. 3a, R-852) reduced the level of *BRLF1* mRNA by 27.7 % after lytic induction with TPA and sodium butyrate (Fig. 3b), indicating the importance of this region in *BRLF1* transcription. Deleting the promoter from position −965 to −388 (Fig. 3a, R-388) and −279 (Fig. 3a, R-279) further reduced the expression to a level about 42.8–52 % of that exhibited by EB-Apr (Fig. 3b). However, a deletion extended to the region that contained the two upstream ZRE sites, from position −965 to −187 (Fig. 3a, R-187), reduced the expression of *BRLF1* mRNA to 21 % of that of EB-Apr (Fig. 3b). Deleting the region between positions −965 and −56 (Fig. 3a, R-56), which yielded a promoter that contained only an Sp1 site and a ZRE (ZRE1) (Fig. 3a), almost totally abolished the transcription and reduced the expression to 14 % of EB-Apr (Fig. 3b). Deleting the region between positions −965 and −42, which resulted in a fragment that contained only one ZRE (ZRE1) (Fig. 3a, R-42) lowered the transcription to 8.4 % of EB-Apr (Fig. 3b). Furthermore, this study demonstrated that activation of *BRLF1* transcription by the transfection of pCMV-Z was more efficient than that activated by TPA and sodium butyrate induction; the amount of mRNA transcribed by EB-Apr after pCMV-Z transfection was nearly sixfold higher than that expressed after TPA and sodium butyrate treatment. The amount of Zta expressed appeared crucial to the transcription of *BRLF1* from the R-42 mutant. Although the amount of *BRLF1* mRNA transcribed from the R-42 mutant was low after TPA and sodium butyrate treatment (Fig. 3b), the transcription was elevated to a level comparable to that exhibited by the mutant strain containing three ZREs after pCMV-Z was transfected (Fig. 3c, R-279). Additionally, transfecting pCMV-Z did not fully activate *BRLF1* transcription if the region between positions −965 and −852 was deleted (Fig. 3c, R-852). Furthermore, immunoblot analysis revealed that decreased *BRLF1* transcription by the mutants also lowered the amount of Rta expressed. R-852 and R-388 mutants produced Rta at a level lower than that of EB-Apr, but higher than those expressed by mutants R-279 and R-187 (Fig. 3d). Meanwhile, mutants R-56 and R-42 produced Rta at levels lower than that expressed by R-279 and R-187 (Fig. 3d). Additionally, the R-852 mutant reduced the production of EBV particles by 64 %; R-388 and R-279 mutants, 74–79 %; R-187, R-56 and R-42 mutants, more than 90 % (Fig. 3e). These results indicated that a slight decrease in *BRLF1* transcription may significantly affect the viral production. The three ZREs in Rp on the EBV genome were also mutated in this study (Fig. 3a). Analysis

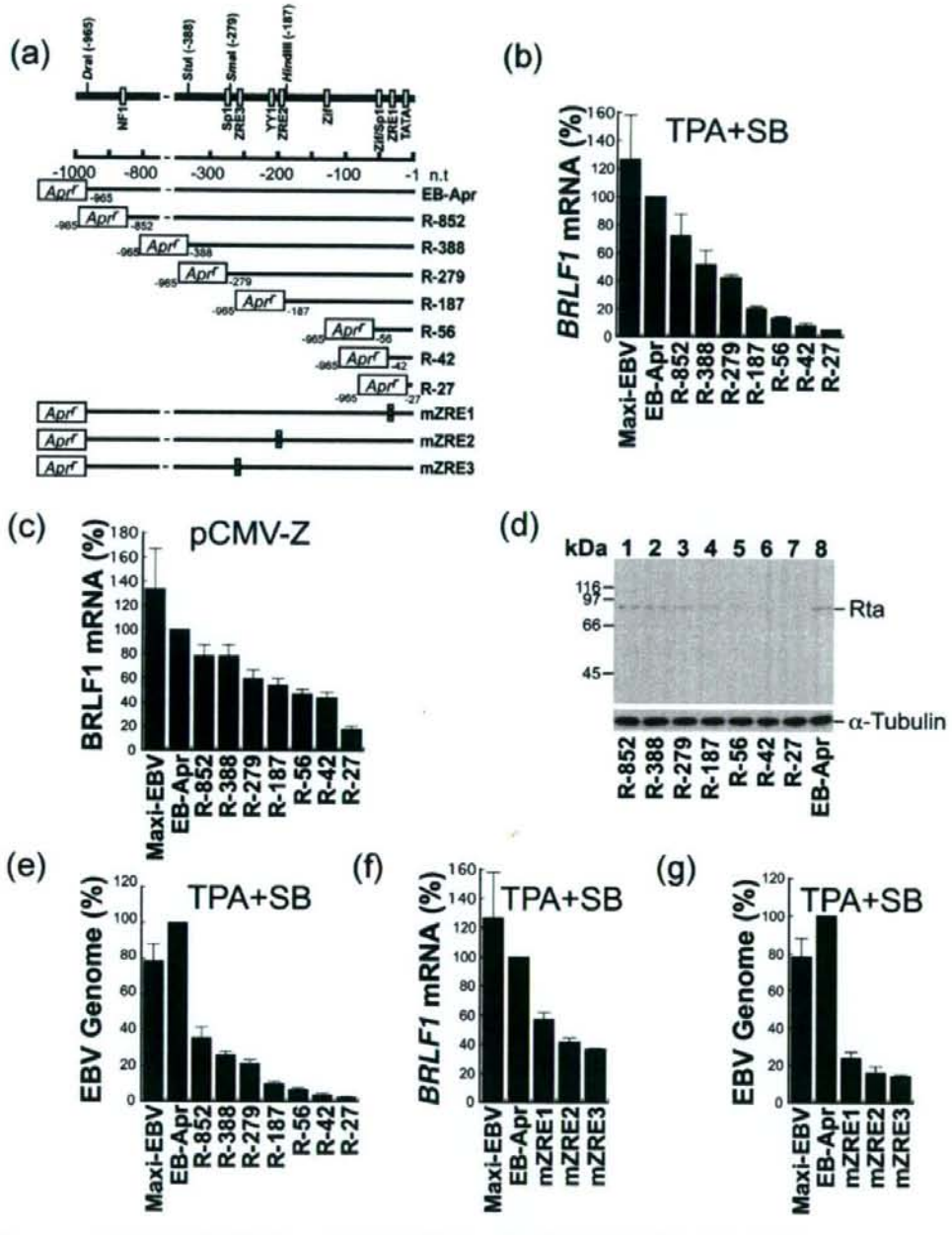

Fig. 3. Mutations in Rp and the influence of the mutations on the transcription of *BRLF1*, expression of Rta and production of EBV particles. Mutations in Rp were generated by the PCR-targeting method (a). NF1, Sp1, YY1, Zif and ZRE denote NF1-, Sp1-, YY1-, Zif268- and Zta-binding sites. An Sp1 site at position −500 is not shown in the figure. The *BRLF1* mRNA in 293 cells was determined by real-time PCR following lytic induction using TPA and sodium butyrate (b) or by transfecting with pCMV-Z (c). Rta that was expressed by the mutants was analysed by immunoblotting (d). EBV particles were collected from the culture medium by centrifugation. The EBV DNA in the viral particles was measured by real-time PCR (e). Transcription of the *BRLF1* mRNA (f) and production of EBV particles (g) by three ZRE mutants, mZRE1, mZRE2 and mZRE3, in the *BRLF1* promoter were also determined. Meanwhile, amounts of *BRLF1* mRNA were normalized with that of *EBNA1* mRNA.

of the *BRLF1* mRNA transcribed by these mutants demonstrated that mutating one of the two upstream ZREs, ZRE2 and ZRE3, lowered the *BRLF1* transcription by 58–63 % and virus production by approximately 84 % after lytic induction with TPA and sodium butyrate. Additionally, mutating ZRE1 also decreased the *BRLF1* transcription by 42.8 % (Fig. 3f) and decreased virus production by 76 % (Fig. 3g).

BDLF1 and *BORF1* mutations

In this work, two mutants, MI-403 and MI-213 (Supplementary Table S1), which contained a mutated *BDLF1* and *BORF1*, respectively, were analysed to determine how these mutations affected capsid assembly. Immunoblot analysis of the proteins in the pellet fraction from the cells that contained maxi-EBV revealed the presence of the BcLF1 (VCA), BORF1 and BDLF1 proteins (Fig. 4a). Additionally, the presence of EBV in the pellet fraction was also verified by real-time PCR (Fig. 4b). Sucrose-gradient centrifugation analysis established that EBV particles generated by maxi-EBV sedimented near the bottom of the gradient (Fig. 4c). Meanwhile, viral capsids assembled by maxi-EBV were also detected within the cell (Fig. 4d). On the other hand, mutants MI-213 and MI-403 did not seem to release EBV capsids into the medium, because immunoblot analysis failed to detect the VCA, BDLF1 and BORF1 proteins in the pellet fractions from the culture medium (Fig. 4a). Meanwhile, assembled EBV capsids, both inside and outside the cell, were undetected by sucrose-gradient sedimentation (Fig. 4c, d). Additionally, transfecting plasmids pHA-BORF1 and pHA-BDLF1 that express BORF1 and BDLF1, respectively, into the cells that contained MI-213 and MI-403, neither complemented the mutations nor restored virus production after lytic induction (Fig. 4e).

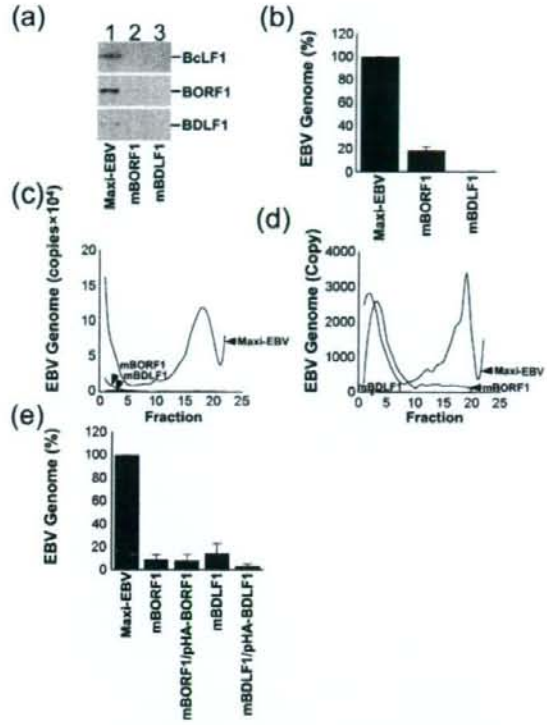

Fig. 4. EBV capsid assembly by mutants with mutations in *BDLF1* and *BORF1*. EBV particles produced by maxi-EBV, mutants that contain a mutation in *BORF1* and *BDLF1*, mBORF1 (MI-213) and mBDLF1 (MI-403), respectively, were collected by centrifugation from the culture medium 5 days following lytic induction. EBV particles in the pellet fraction were detected by immunoblotting using anti-BcLF1, anti-BORF1 and anti-BDLF1 antibodies (a). EBV DNA packaged in the virion was determined by real-time PCR (b). EBV capsids both in the medium (c) and inside the cells (d) were subjected to 20–60 % sucrose-gradient sedimentation analysis. Cells that contained mBDLF1 and mBORF1 were transfected with pHA-BDLF1 and pHA-BORF1, respectively. EBV particles that were produced by these cells were analysed using real-time PCR (e).

DISCUSSION

This investigation employed EZ::TN <KAN-2> and generated about 50 000 EBV mutants *in vitro* using 1 μg maxi-EBV DNA. These mutants can be screened randomly for mutations associated with a particular phenotype, but screening them indiscriminately is impractical. Therefore, a mutant library was established to facilitate genetic studies. To establish such a mutant library, mutants were randomly selected from a mutant pool and the location of the insertions was determined by DNA sequencing. Multiple insertions of the transposon into the EBV genome were occasionally found, probably owing to a lack of transposition immunity of EZ::TN <KAN-2>; these mutants were later eliminated. Finally, sequencing analysis revealed that among the 93 annotated EBV genes, 60 were mutated. Since identifying a mutation in the remaining 33 genes that lack a transposon insertion in a large pool of mutants was time-consuming, a PCR-targeting method (Datsenko & Wanner, 2000; Gust *et al.*, 2003) was subsequently used to mutate particular genes on the EBV genome. This approach efficiently mutates the EBV genome. The recombination method and transposon mutagenesis generated an EBV mutant library that contains 249 mutants (Fig. 1; Supplementary Table S1). The λ-RED recombinase system is known to promote recombination between a linear double-stranded DNA and its target DNA (Murphy, 1998). This fact may explain why the frequency of deletion caused by intra-DNA recombination following PCR targeting is not particularly high. The integrity of the EBV genome was examined using restriction digestion following transposon mutagenesis and PCR targeting; the mutants that contained a detectable deletion were thus